Geochronology, 4, 191–211, 2022
https://doi.org/10.5194/gchron-4-191-2022

Cosmogenic ages indicate no MIS 2 refugia in the Alexander Archipelago, Alaska

Caleb K. Walcott[1], Jason P. Briner[1], James F. Baichtal[2], Alia J. Lesnek[3], and Joseph M. Licciardi[4]

[1]Department of Geology, University at Buffalo, Buffalo, NY 14260, USA
[2]Tongass National Forest, Thorne Bay, AK 99919, USA
[3]School of Earth and Environmental Sciences, CUNY Queens College, Flushing, NY 11367, USA
[4]Department of Earth Sciences, University of New Hampshire, Durham, NH 03824, USA

Correspondence: Caleb K. Walcott (ckwalcot@buffalo.edu)

Received: 9 November 2021 – Discussion started: 15 November 2021
Revised: 15 March 2022 – Accepted: 18 March 2022 – Published: 7 April 2022

Abstract. The late-Pleistocene history of the coastal Cordilleran Ice Sheet remains relatively unstudied compared to chronologies of the Laurentide Ice Sheet. Yet accurate reconstructions of Cordilleran Ice Sheet extent and the timing of ice retreat along the Pacific Coast are essential for paleoclimate modeling, assessing meltwater contribution to the North Pacific, and determining the availability of ice-free land along the coastal Cordilleran Ice Sheet margin for human migration from Beringia into the rest of the Americas. To improve the chronology of Cordilleran Ice Sheet history in the Alexander Archipelago, Alaska, we applied ^{10}Be and ^{36}Cl dating to boulders and glacially sculpted bedrock in areas previously hypothesized to have remained ice-free throughout the local Last Glacial Maximum (LLGM; 20–17 ka). Results indicate that these sites, and more generally the coastal northern Alexander Archipelago, became ice-free by 15.1 ± 0.9 ka ($n = 12$ boulders; 1 SD). We also provide further age constraints on deglaciation along the southern Alexander Archipelago and combine our new ages with data from two previous studies. We determine that ice retreated from the outer coast of the southern Alexander Archipelago at 16.3 ± 0.8 ka ($n = 14$ boulders; 1 SD). These results collectively indicate that areas above modern sea level that were previously mapped as glacial refugia were covered by ice during the LLGM until between ~ 16.3 and 15.1 ka. As no evidence was found for ice-free land during the LLGM, our results suggest that previous ice-sheet reconstructions underestimate the regional maximum Cordilleran Ice Sheet extent, and that all ice likely terminated on the continental shelf. Future work should investigate whether presently submerged areas of the continental shelf were ice-free.

1 Introduction

The late-Pleistocene history of the coastal Cordilleran Ice Sheet remains relatively unstudied compared to chronologies of the Laurentide Ice Sheet (Dalton et al., 2020). Cordilleran Ice Sheet margin reconstructions from the Pacific Coast are based largely on qualitative field observations with little chronologic control (Dyke, 2004; Carrara et al., 2007; Dalton et al., 2020). While a few studies have recently generated local ice sheet retreat chronologies from terrestrial locations along the Pacific Coast (Darvill et al., 2018; Lesnek et al., 2018, 2020), there are still large areas of the southeastern Alaskan coastline that lack direct age constraints on deglaciation (Fig. 1). Much of the Northern Hemisphere was covered by continental ice sheets during the global Last Glacial Maximum (GLGM; ~ 26–19 ka; Clark et al., 2009). Chronologies of northern hemispheric glaciation have revealed that while the Laurentide Ice Sheet and many alpine glaciers worldwide were at their greatest extents during the GLGM, the coastal Cordilleran Ice Sheet and the Puget Lobe reached their maximum size ~ 20–17 cal ka (local Last Glacial Maximum; hereafter LLGM; Porter and Swanson, 1998; Booth et al., 2003; Praetorius and Mix, 2014; Darvill et al., 2018; Lesnek et al., 2018). Other studies have also explored the Cordilleran Ice Sheet contributions to meltwater pulse 1A (~ 14.6 ka) following the saddle collapse between the Laurentide Ice Sheet and Cordilleran Ice Sheet (Gregoire et

al., 2016; Ivanovic et al., 2017). Improved constraints on Cordilleran Ice Sheet history around the time of meltwater pulse 1A are necessary to elucidate any influences of coastal Cordilleran Ice Sheet configuration and retreat on saddle collapse. Additionally, numerical modeling studies show differing responses of the Cordilleran Ice Sheet to last deglacial climate oscillations, thus highlighting the need for an improved Cordilleran Ice Sheet chronology to bolster model improvement and validation (Tarasov et al., 2012; Seguinot et al., 2014; Gregoire et al., 2016; Seguinot et al., 2016; Ivanovic et al., 2017). Finally, a temporally accurate paleogeographic reconstruction of the coastal Cordilleran Ice Sheet margin is required to assess whether a viable coastal route existed for early Americans migrating from Beringia into the Americas. This route hinges on the presence of ice-free land (refugia) suitable for human habitation during the migration event(s). Earlier mapping efforts and other supporting information indicate areas of potential refugia along the former coastal Cordilleran Ice Sheet margin (Demboski et al., 1999; Cook et al., 2001; Carrara et al., 2003, 2007; Shafer et al., 2010, 2011; Hebda et al., 2022).

This study has two goals: (1) improve the spatio-temporal patterns of coastal Cordilleran Ice Sheet deglaciation in southeastern Alaska and (2) assess whether areas of the northern Alexander Archipelago mapped as refugia were ice-free throughout the LLGM and thus available for human habitation (Fig. 2). We report 25 new cosmogenic ^{10}Be exposure ages from boulders and bedrock in the northern Alexander Archipelago – the first exposure ages documenting Cordilleran Ice Sheet retreat from this coastal region. We also report four ^{10}Be and four cosmogenic ^{36}Cl ages from Suemez Island in the southern Alexander Archipelago. Our data constrain the deglaciation of the marine-terminating Cordilleran Ice Sheet margin and expand the overall North Pacific coastal glacial chronology. Our results suggest deglaciation of coastal regions $\sim$ 15.4–14.8 ka in the northern Alexander Archipelago and do not support previous mapping of refugia in areas that are presently above sea level.

2 Setting

The Alexander Archipelago, southeastern Alaska, stretches $\sim$ 480 km (Fig. 2) along the western coast of British Columbia. The southern part of the archipelago is dominated by Prince of Wales Island and surrounding islands, whereas the northern part encompasses Baranof Island and Chichagof Island and a collection of smaller islands. The Alexander Archipelago consists of accreted terranes (Triassic to Cretaceous in age) with quartz-bearing diorite and granodiorite units and notable Eocene–Miocene granitic intrusive complexes (Wilson et al., 2015). Late-Pleistocene volcanic activity on southern Kruzof Island formed the Mt. Edgecumbe volcanic field (Riehle, 1996). Post-LLGM (late-Pleistocene and Holocene) eruptions formed extensive andesite flows on the island and blanketed much of the surrounding area with tephra (Riehle et al., 1984, 1992; Riehle, 1996). Modern climate of the Alexander Archipelago is dominated by cool, wet summers and mild winters, with perennial heavy rainfall – Sitka (Baranof Island) receives $\sim$ 2200 mm yr^{-1} while Chichagof Island receives over 3300 mm yr^{-1} (Ager, 2019; https://wrcc.dri.edu/summary/Climsmak.html, last access: 14 March 2022). Snowfall is minimal at lower elevations but more substantial in higher-elevation areas (https://wrcc.dri.edu/summary/Climsmak.html). Glaciers occupy alpine cirques in the Alexander Archipelago (totaling < 150 km^2), primarily on Baranof and Chichagof islands (Molnia, 2008). Presently, low-elevation (< 700 m a.s.l.) areas of the archipelago are dominated by coniferous rainforests, while alpine tundra exists above the tree line (> 700 m a.s.l.; Ager, 2019).

Previous mapping shows much, if not all, of southeastern Alaska covered by the Cordilleran Ice Sheet during the LLGM and the last deglaciation, with a maximum position likely terminating several kilometers out on the continental shelf of the Gulf of Alaska (Carrara et al., 2007). Ice caps formed atop the Coast Mountains and high massifs of the Alexander Archipelago coalesced and flowed westward to the continental shelf and the Pacific Ocean (Capps, 1932; Mann, 1986; Mann and Hamilton, 1995). Outlet glaciers occupied the present fjord and strait landscape (Carrara et al., 2007). Today, the landscape is strewn with clear indicators of widespread glaciation including deep fjords, glacially sculpted bedrock draped with boulders, and a variety of other glacial landforms, but it remains unclear whether all of southeastern Alaska was covered by the Cordilleran Ice Sheet during the LLGM. Some areas of the Alexander Archipelago, presently above sea level, are hypothesized to have been ice-free throughout the LLGM (Carrara et al., 2007). Recent studies using ^{10}Be surface exposure dating of glacial landforms, however, indicate that some of these purported ice-age refugia in the southern Alexander Archipelago were covered by the Cordilleran Ice Sheet during its LLGM advance (Lesnek et al., 2018). Other areas previously mapped as ice age refugia in the northern Alexander Archipelago (Carrara et al., 2007; Dalton et al., 2020) are investigated in this study; if their presence is confirmed with numerical dating techniques, this would be a significant confirmation of the existence of coastal refugia.

3 Methods

3.1 Boulder and bedrock sampling

We collected 29 samples (11 bedrock, 18 boulder) for cosmogenic ^{10}Be surface exposure dating (hereafter ^{10}Be dating) during summer 2018, 2019, and 2020 (Figs. 3 and 4) from several sites in coastal southeastern Alaska, including Suemez ($n = 4$), Baranof ($n = 11$), Biorka ($n = 4$), Kruzof

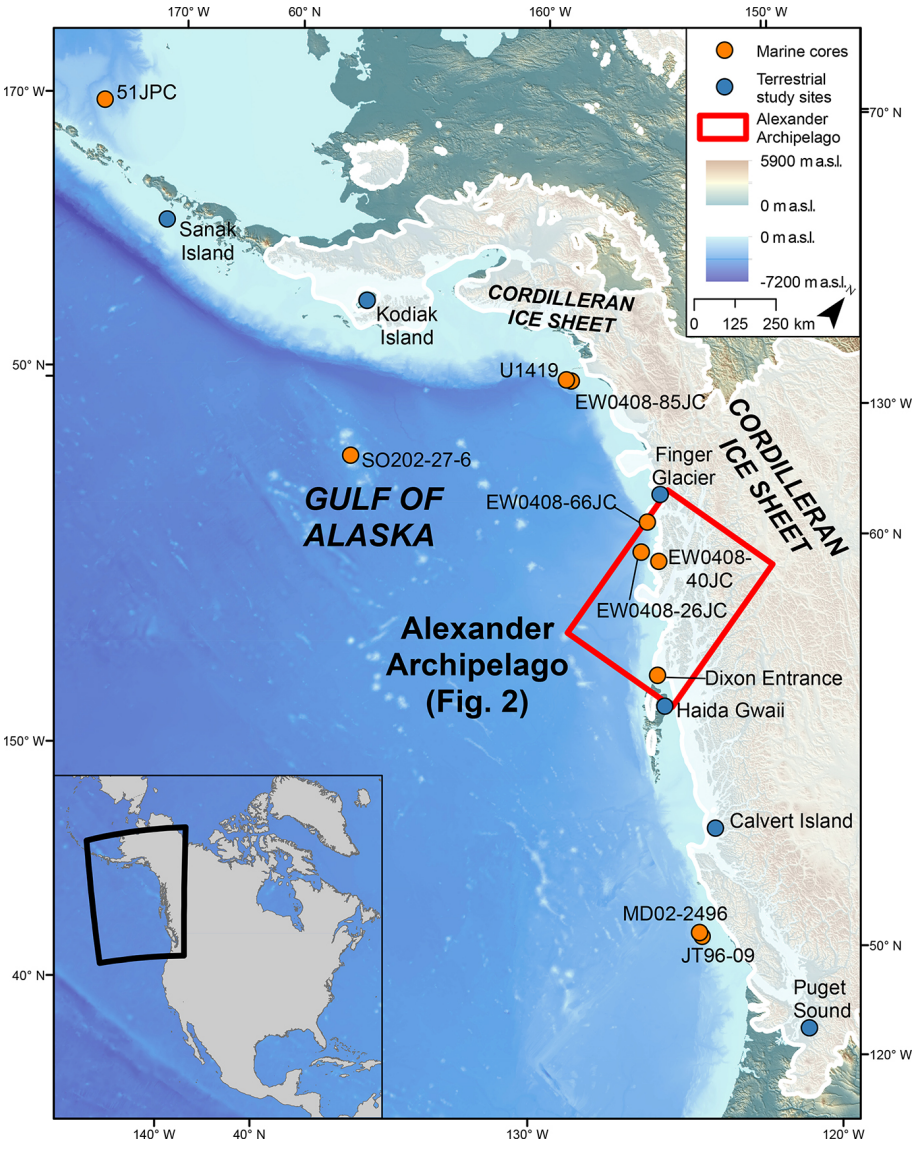

Figure 1. Map of the North Pacific region showing ice limits at 18.0 ka from Dalton et al. (2020) with location of relevant sites mentioned in the text. The Alexander Archipelago is highlighted by the red box on the main figure. Orange dots indicate locations of marine sediment cores: 51-JPC (Caissie et al., 2010), SO202-27-6 (Maier et al., 2018), U1419 (Walczak et al., 2020), EW0408-85JC (Davies et al., 2011; Praetorius and Mix, 2014, Praetoruis et al., 2015), EW0408-66JC (Praetorius and Mix, 2014; Praetorius et al., 2016), EW0408-26JC (Praetorius and Mix, 2014; Praetorius et al., 2016), EW0408-40JC (Addison et al., 2010), MD02-2496 (Cosma et al., 2008), and JT96-09 (Kienast and McKay, 2001). Blue dots indicate location of terrestrial study sites: Sanak Island (Misarti et al., 2012), Kodiak Island (Mann and Peteet, 1994), Finger Glacier (Mann, 1986), Haida Gwaii (Clague et al., 1982; Mathewes and Clague, 2017), Calvert Island (Darvill et al., 2018), and Puget Sound (Porter and Swanson, 1998).

($n = 4$) and Chichagof ($n = 6$) islands. Our samples range in elevation from ~ 50 to ~ 930 m a.s.l.; all sites are above the local marine limits of ~ 10–20 m a.s.l. (Baichtal et al., 2021). We preferentially sampled paired sites consisting of stable boulders and neighboring unvegetated bedrock surfaces. This strategy allowed us to assess whether bedrock surfaces contain isotopic inheritance and provides insights into ice-sheet erosion history. In the absence of suitable boulders at a few locations, we sampled bedrock with clear evidence of glacial erosion to mitigate the possibility of ^{10}Be inheritance.

We also collected samples from four glacially transported boulders on the southwestern portion of Suemez Island for ^{36}Cl surface exposure dating during the summer 2019 field season (Figs. 5, 6; Table 2). The boulders consist of non-vesicular olivine basalt of "Tertiary to Quaternary" age (Eberlein et al., 1983).

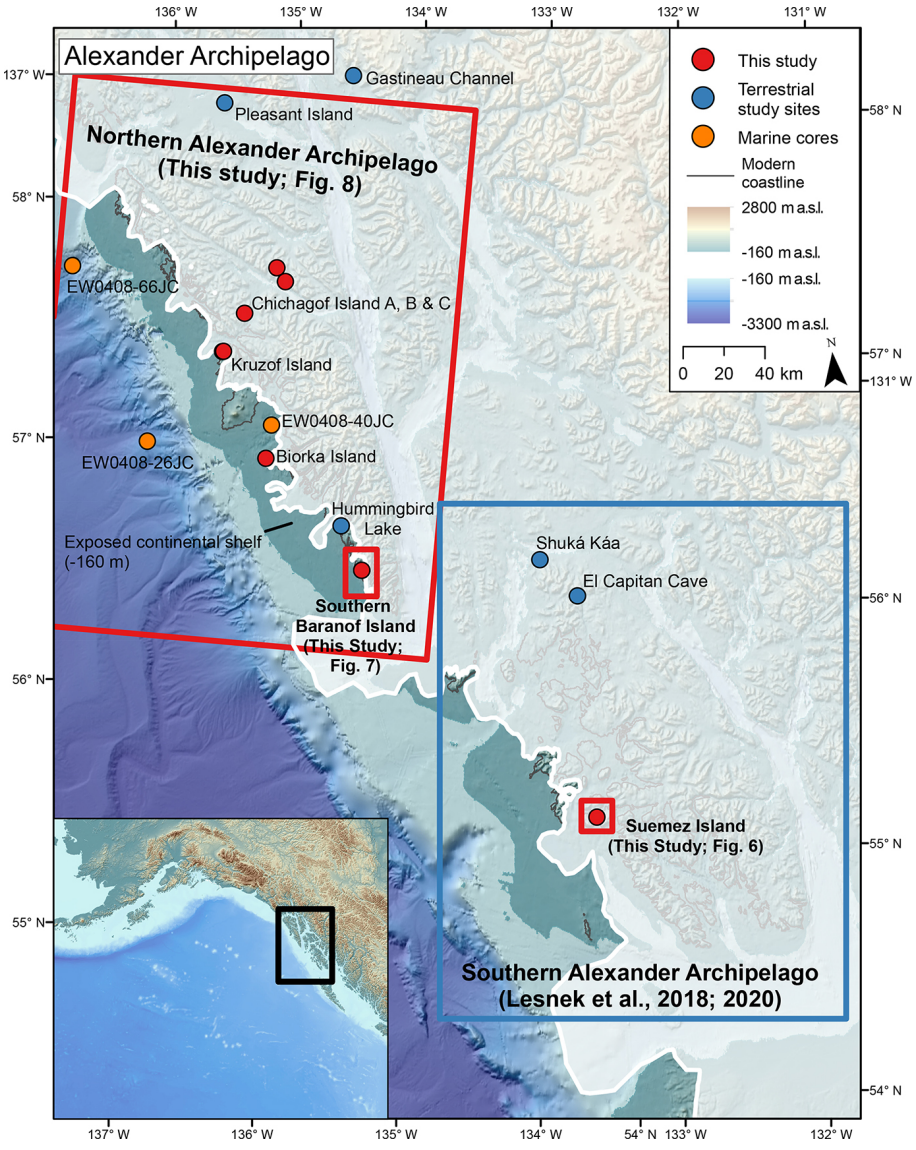

Figure 2. The Alexander Archipelago showing relevant marine sediment cores and terrestrial chronologies. Shaded white areas show hypothesized LLGM Cordilleran Ice Sheet extent (Lesnek et al., 2020). −160 m relative sea level lowering after Baichtal et al. (2021). Red boxes and points show sampling locations from this study. Blue box shows extent of study area from Lesnek et al. (2018, 2020). Orange dots represent locations of marine sediment cores: EW0408-66JC and EW0408-26J (Praetorius and Mix, 2014; Praetorius et al., 2016) and EW0408-40JC (Addison et al., 2010). Blue dots indicate locations of relevant terrestrial study sites: Gastineau Channel (Miller, 1973), Pleasant Island (Hansen and Engstrom, 1996), Hummingbird Lake (Ager, 2019), Shuká Káa (Lesnek et al., 2018), and El Capitan Cave (Wilcox et al., 2019).

Surface samples were collected from the upper few centimeters of the boulders and bedrock using a handheld angle grinder, hammer, and chisel. We avoided sampling areas of the boulder tops and bedrock surfaces with visible signs of surface erosion (e.g., fractures, weathering pits). We did, however, observe erosional features on the boulders sampled for ^{36}Cl dating. We avoided collecting material from these areas, instead sampling parts of the basaltic boulder tops that showed fresh, unweathered surfaces. We recorded sample locations with a handheld GPS unit or GAIA GPS (both with a vertical uncertainty of ±5 m) and measured topographic shielding in the field with a clinometer and compass.

3.2 ^{10}Be dating

We processed samples at the University at Buffalo Cosmogenic Isotope Laboratory following established quartz purification and beryllium extraction procedures (e.g., Corbett et al., 2016). After quartz purification, we dissolved samples in hydrofluoric acid with precisely weighed ^{9}Be car-

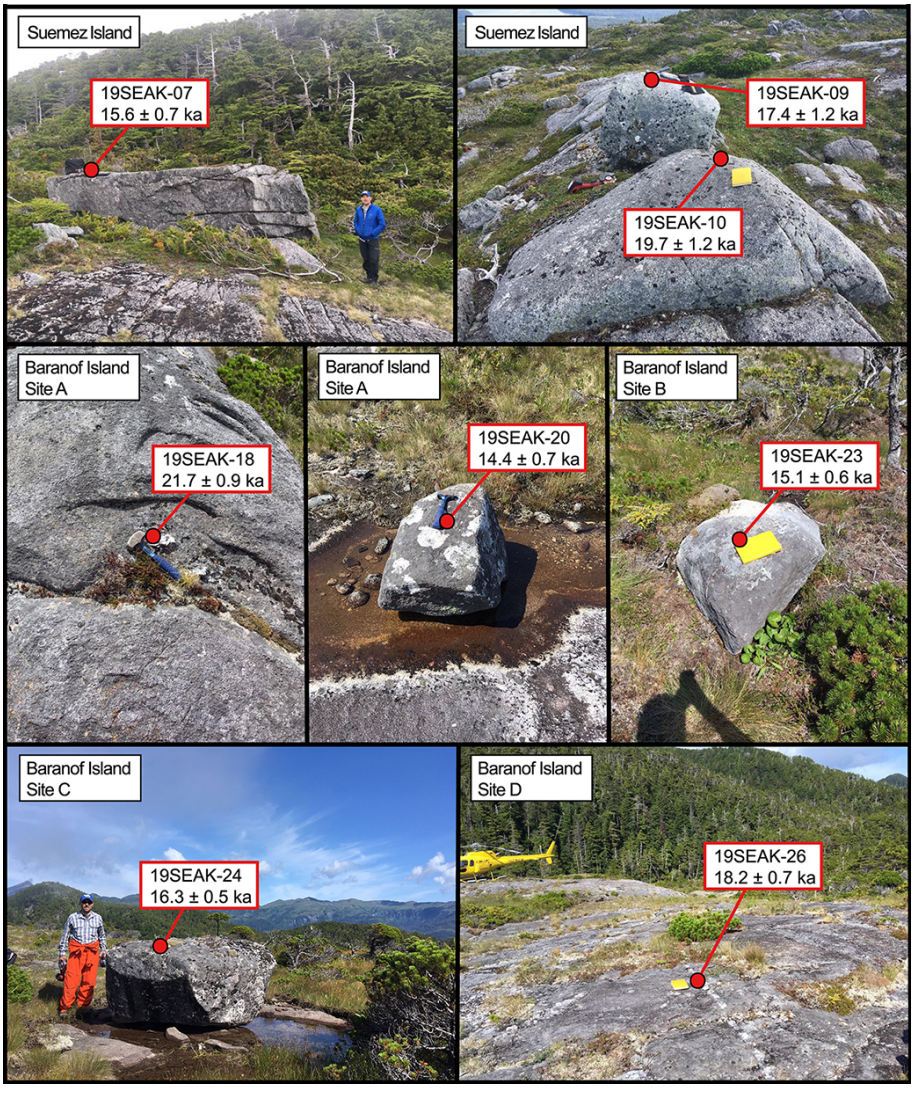

Figure 3. Sample photos from 2019 field season. All ^{10}Be ages shown with 1σ internal uncertainty.

rier (PRIME Lab 2017.11.17-Be #3/#4; ^{9}Be concentration of 1074 ± 8 ppm). We isolated, oxidized, and packed beryllium into target cathodes in five different batches for accelerator mass spectrometer (AMS) analysis at PRIME lab at Purdue University. The samples were measured with respect to the 07KNSTD standard (^{10}Be / ^{9}Be ratio of 2.85×10^{-12}; Nishiizumi et al., 2007). We corrected sample ratios using batch-specific blank values between 7.50×10^{-16} and 3.14×10^{-15}. AMS analytical uncertainty ranged from 3.2 % to 7.3 % with an average value of 4.7 %.

We calculated all ^{10}Be ages using version 3 of the CRONUS-Earth exposure age calculator (http://hess.ess.washington.edu, last access: 14 March 2022; Balco et al., 2008; Balco, 2017), using the Arctic production rate (Young et al., 2013) and a time-dependent (Lm) scaling scheme (Lal, 1991).

3.3 ^{36}Cl dating

All whole rock samples were prepared at the University of New Hampshire Cosmogenic Isotope Laboratory using a modified version of the protocols in Stone et al. (1996) and Licciardi et al. (2008). After samples were crushed, etched in nitric acid, and homogenized, total sample chloride was measured on a ∼ 1 g aliquot of rock that was spiked with a small amount of ^{37}Cl-enriched solution (LLNL Spike A; ^{35}Cl / ^{37}Cl = 0.93; 1285 ± 3 ppm Cl) and a carrier containing ∼ 4000 µg of Br. Cl was extracted as Ag(Cl,Br) following standard procedures, and chlorine concentrations were determined through isotope dilution of ^{35}Cl / ^{37}Cl ratios (Faure, 1986). ^{36}Cl was extracted from full rock samples as Ag(Cl,Br) after adding a carrier containing ∼ 4800 µg of Br and a natural ratio Cl carrier (^{35}Cl / ^{37}Cl = 3.127; 1436 ± 9 ppm Cl) to increase the size of the final precipitate.

Figure 4. Sample photos from 2018 and 2020 field season. All ^{10}Be ages are shown with 1σ internal uncertainty. Note the relatively small size of 20SEAK-15.

^{35}Cl / ^{37}Cl and ^{36}Cl / Cl ratios were measured at the Center for Accelerator Mass Spectrometry at Lawrence Livermore National Laboratory. Analytical uncertainty on ^{35}Cl / ^{37}Cl measurements ranged from 0.04 % to 0.43 %; analytical uncertainty on ^{36}Cl / Cl measurements ranged from 2.12 % to 2.87 %. Major and trace element analyses were conducted by SGS Minerals Services in Burnaby, British Columbia, Canada. Reported total Cl and ^{36}Cl concentrations are corrected for batch-specific process blanks (Table 2). Analytical data used to determine surface exposure ages are provided in Tables S1 and S2 in the Supplement. ^{36}Cl exposure ages were calculated using an online exposure age calculator (http://stoneage.ice-d.org/math/Cl36/v3/v3_Cl36_age_in.html, last access: 14 March 2022) and Lm scaling (Lal, 1991).

3.4 Exposure age calculation considerations

We made no corrections for post-glacial elevation changes or snow cover when calculating our ^{10}Be and ^{36}Cl ages. Post-glacial isostatic adjustment results in a time-varying rate of cosmogenic nuclide production (Jones et al., 2019). This effect can be corrected for using comprehensive records of regional emergence constrained by glacial isostatic adjustment models or relative sea-level histories. Hundreds of radiocarbon ages constrain the relative sea level chronology in the Alexander Archipelago; the sites in our study experienced

Figure 5. Basalt samples and ^{36}Cl ages from southwestern Suemez Island. Ages are reported at 1σ internal uncertainty.

$\sim$ 50 m of relative sea level lowering due to forebulge collapse between $\sim$ 15 and 10 ka (Baichtal et al., 2021). Corrections for glacial isostatic adjustment history, albeit slightly uncertain given site-to-site differences in elevation history, result in small changes ($\sim$ 1 % age decrease), and thus we report our ages without any correction for isostatic adjustment (Tables 1 and 2). Furthermore, changes in air pressure near a retreating ice margin and shifts in air compression above a sample site that experienced elevation change may mitigate any effects of isostatic adjustment on cosmogenic nuclide production, potentially rendering any elevation correction unnecessary (Staiger et al., 2007).

Extended periods of thick and dense snow cover can also inhibit ^{10}Be and ^{36}Cl production in a rock surface and lead to erroneously young apparent exposure ages. While modern snowfall reports for lower-elevation areas of the Alexander Archipelago indicate minimal average wintertime snow cover (10–20 cm; https://wrcc.dri.edu/summary/Climsmak.html), there are no data for higher-elevation areas. Consequently, we cannot report our ages with reliable snow shielding corrections and these exposure dates should be considered minimum ages. However, most of our sites are from low to moderate elevations (< 500 m a.s.l.; Table 1).

Post-depositional weathering and erosion can also affect exposure ages. We observed fresh, unweathered glacially scoured bedrock across all our field sites, indicating minimal post-glacial erosion. We made no corrections for erosion in our age calculations presented within the article text, and thus these should be considered minimum ages. For sensitivity purposes, we calculated ages using an erosion rate of 0.3 cm kyr^{-1}, similar to erosion rates applied nearby in British Columbia (Menounos et al., 2017). These erosion-corrected ages are between 2 % and 7 % older and are found in Tables S3 and S4.

Both cosmogenic and nucleogenic ^{36}Cl can be present in rock surfaces, and for our surface exposure age calculations we assumed steady-state production/decay of nucleogenic ^{36}Cl. Moderate amounts of nucleogenic ^{36}Cl are produced when ^{35}Cl absorbs neutrons released by the decay of U and Th isotopes (Gosse and Phillips, 2001). However, because the formation age of the sampled basalt flow on Suemez Island is loosely constrained to the "Tertiary to Quaternary" (Eberlein et al., 1983), nucleogenic ^{36}Cl production/decay may or may not be in steady state. To assess the sensitivity of our exposure ages to the assumption of steady-state nucleogenic ^{36}Cl production, we also calculated exposure ages using a rock formation age of 20 ka, which, given the timing of the LLGM ice advance in southeastern Alaska (Lesnek et al., 2018), is the youngest formation age we might expect for these rocks. Results of this test (Table S3) show that calculated ^{36}Cl ages are relatively insensitive to rock formation age (< 1 % surface exposure age increase in all cases), which is well within total uncertainty.

4 Results

We sampled from the summit of a massif at $\sim$ 410 m a.s.l. on south-central Suemez Island (southern Alexander

https://doi.org/10.5194/gchron-4-191-2022

Table 1. ^{10}Be surface exposure age data.

Sample ID	Sample type	Latitude (° N)[a]	Longitude (° W)[a]	Elevation (m a.s.l.)[a]	Boulder height (m)	Sample thickness (cm)	Topographic shielding correction	Quartz (g)	^{9}Be added (µg)	^{10}Be / ^{9}Be ratio[b]	^{10}Be / ^{9}Be ratio uncertainty	^{10}Be (atoms g^{-1})	^{10}Be uncertainty (atoms g^{-1})	^{10}Be age (ka)[c] Arctic PR	^{10}Be age (ka)[c] global PR
Biorka Island															
18JB005	Boulder	56.8482	−135.5314	47	1.0	3.0	1.0000	34.37	232	1.36E−13	4.38E−15	6.60E+04	2.12E+03	15.3 ± 0.5 (0.8)	14.7 ± 0.5 (1.2)
18JB006	Boulder	56.8471	−135.5315	43	1.2	3.0	1.0000	34.57	221	1.32E−13	4.87E−15	6.40E+04	2.35E+03	14.9 ± 0.6 (0.8)	14.3 ± 0.5 (1.2)
18JB007	Boulder	56.8527	−135.5363	46	1.0	3.0	1.0000	33.92	233	1.35E−13	4.54E−15	6.60E+04	2.23E+03	15.4 ± 0.5 (0.8)	14.8 ± 0.5 (1.1)
18JB008	Boulder	56.8528	−135.5362	46	1.0	3.0	1.0000	24.35	232	8.60E−14	2.92E−15	5.90E+04	1.99E+03	13.7 ± 0.5 (0.7)	13.2 ± 0.4 (1.1)
Suemez Island															
19SEAK-07	Boulder	55.2469	−133.3414	376	2.0	2.0	0.9958	21.24	233	1.25E−13	5.41E−15	9.19E+04	3.97E+03	15.6 ± 0.7 (0.9)	14.9 ± 0.6 (1.3)
19SEAK-08	Boulder	55.2470	−133.3419	392	1.0	2.0	0.9984	12.04	226	7.20E−14	5.42E−15	9.03E+04	6.80E+03	15.0 ± 1.1 (1.3)	14.4 ± 1.1 (1.5)
19SEAK-09	Boulder	55.2477	−133.3406	394	0.7	2.0	1.0000	19.44	233	1.31E−13	9.28E−15	1.05E+05	7.44E+03	17.4 ± 1.2 (1.4)	16.7 ± 1.2 (1.7)
19SEAK-10	Bedrock	55.2477	−133.3406	419	–	3.0	1.0000	17.81	213	1.38E−13	8.63E−15	1.21E+05	7.55E+03	19.7 ± 1.2 (1.4)	18.9 ± 1.2 (1.9)
Baranof Island															
Site A															
19SEAK-17	Boulder	55.3677	−134.9015	140	0.5	2.0	0.9923	25.08	233	1.30E−13	6.21E−15	8.02E+04	3.84E+03	16.9 ± 0.8 (1.0)	16.3 ± 0.8 (1.5)
19SEAK-18	Bedrock	56.3723	−134.9084	129	–	2.0	1.0000	25.24	232	1.66E−13	6.95E−15	1.02E+05	4.27E+03	21.7 ± 0.9 (1.2)	20.8 ± 0.9 (1.8)
19SEAK-19	Bedrock	56.3718	−134.9094	126	–	2.0	1.0000	24.80	233	2.10E−13	8.06E−15	1.31E+05	5.05E+03	28.0 ± 1.1 (1.5)	26.9 ± 1 (2.3)
19SEAK-20	Boulder	56.3712	−134.9082	135	0.6	2.0	1.0000	25.03	233	1.09E−13	5.59E−15	6.80E+04	3.47E+03	14.4 ± 0.7 (0.9)	13.8 ± 0.7 (1.3)
Site B															
19SEAK-21	Boulder	56.3636	−134.9068	48	0.5	2.0	1.0000	25.05	233	1.00E−13	4.57E−15	6.23E+04	2.84E+03	14.4 ± 0.7 (0.9)	13.8 ± 0.6 (1.2)
19SEAK-22	Bedrock	56.3636	−134.9072	58	–	2.0	0.9749	20.17	230	8.03E−14	3.10E−15	6.13E+04	2.36E+03	14.4 ± 0.6 (0.8)	13.8 ± 0.5 (1.2)
19SEAK-23	Boulder	56.3638	−134.9092	68	0.5	2.0	0.9911	20.24	231	8.64E−14	3.29E−15	6.60E+04	2.51E+03	15.1 ± 0.6 (0.8)	14.5 ± 0.6 (1.2)
Site C															
19SEAK-24	Boulder	56.3228	−134.892	150	1.0	1.5	1.0000	20.12	234	1.01E−13	3.39E−15	7.83E+04	2.63E+03	16.3 ± 0.5 (0.8)	15.6 ± 0.5 (1.3)
19SEAK-25	Bedrock	56.3231	−134.8916	163	–	1.5	1.0000	19.99	234	9.80E−14	3.41E−15	7.68E+04	2.67E+03	15.7 ± 0.6 (0.8)	15.1 ± 0.5 (1.3)
Site D															
19SEAK-26	Bedrock	56.3554	−134.8856	145	–	2	0.9879	25.12	235	1.37E−13	5.54E−15	8.56+04	3.47E+03	18.2 ± 0.7 (1.0)	17.4 ± 0.7 (1.5)
19SEAK-27	Bedrock	56.3555	−134.8855	142	–	1.5	0.9963	25.04	233	1.54E−13	5.89E−15	9.59E+04	3.67E+03	20.2 ± 0.8 (1.1)	19.3 ± 0.7 (1.6)
Kruzof Island															
20SEAK-7	Boulder	57.3112	−135.8126	558	2.5	1.5	0.9976	20.14	233	1.36E−13	7.24E−15	1.05E+05	5.59E+03	14.9 ± 0.8 (1.0)	14.3 ± 0.8 (1.3)
20SEAK-10	Bedrock	57.3112	−135.8111	559	–	1.5	0.96912	20.13	231	1.20E−13	8.48E−15	9.23E+04	6.50E+03	13.4 ± 1.0 (1.1)	12.9 ± 0.9 (1.3)
20SEAK-12	Boulder	57.3110	−135.8110	569	1.0	1.0	0.9927	20.07	382	8.32E−14	3.74E−15	1.06E+05	4.77E+03	14.9 ± 0.7 (0.9)	14.3 ± 0.6 (1.3)
20SEAK-13	Boulder	57.3109	−135.8109	568.3	1.5	1.0	0.9941	20.25	230	1.36E−13	7.43E−15	1.04E+05	5.65E+03	14.6 ± 0.8 (1.0)	14.1 ± 0.8 (1.3)
Chichagof Island															
Site A															
20SEAK-14	Bedrock	57.4621	−135.6354	476	–	0.5	1.0000	20.25	230	1.34E−13	6.34E−15	1.01E+05	4.80E+03	15.3 ± 0.7 (0.9)	14.6 ± 0.7 (1.3)
20SEAK-15	Boulder	57.4621	−135.6354	476	0.3	1.0	1.0000	20.33	227	1.13E−13	6.04E−15	8.38E+04	4.50E+03	12.7 ± 0.7 (0.8)	12.2 ± 0.7 (1.1)
20SEAK-16	Boulder	57.4618	−135.6351	473	0.3	1.5	1.0000	20.26	240	7.48E−14	4.78E−15	5.92E+04	3.78E+03	9.0 ± 0.6 (0.7)	8.6 ± 0.6 (0.9)

Table 1. Continued.

Sample ID	Sample type	Latitude (° N)[a]	Longitude (° W)[a]	Elevation (m a.s.l.)[a]	Boulder height (m)	Sample thickness (cm)	Topographic shielding correction	Quartz (g)	^{9}Be added (µg)	^{10}Be / ^{9}Be ratio[b]	^{10}Be / ^{9}Be ratio uncertainty	^{10}Be (atoms g^{-1})	^{10}Be uncertainty (atoms g^{-1})	^{10}Be age (ka)[c] Arctic PR	^{10}Be age (ka)[c] global PR
Site B															
20SEAK-18	Boulder	57.5743	−135.2721	817	0.5	3.0	1.0000	15.20	226	1.09E−13	7.99E−15	1.09E+05	7.99E+03	12.4 ± 0.9 (1.0)	11.8 ± 0.9 (1.2)
20SEAK-19	Bedrock	57.5743	−135.2720	816	–	1.5	1.0000	20.05	239	1.57E−13	7.31E−15	1.25E+05	5.81E+03	14.1 ± 0.7 (0.8)	13.5 ± 0.6 (1.2)
Site C															
20SEAK-22	Bedrock	57.6425	−135.3483	779	–	2.0	1.0000	20.12	231	1.98E−13	8.58E−15	1.52E+05	6.59E+03	17.7 ± 0.8 (1.0)	17.0 ± 0.7 (1.5)

[a] Elevations and positions were recorded with a Garmin handheld GPS receiver (∼ 5 m vertical uncertainty) or GAIA GPS (∼ 5 m vertical uncertainty). [b] AMS results from PRIME Lab are standardized to 07KNSTD (Nishiizumi et al., 2007); ratios are blank corrected and shown at 1 SD uncertainty. [c] ^{10}Be ages reported with 1σ internal uncertainties; external uncertainties in parentheses; calculated with CRONUS-Earth calculator v. 3 (Balco et al., 2008) using the Arctic production rate (Young et al., 2013) or global production rate (Borchers et al., 2016) and Lm scaling.

Table 2. ^{36}Cl surface exposure age data.

Sample ID	Sample type	Latitude (° N)[a]	Longitude (° W)[a]	Elevation (m a.s.l.)[a]	Boulder height (m)	Sample thickness (cm)	Density (g cm^{-3})	Topographic shielding correction	Aliquot dissolved for total Cl determination (g)	^{37}Cl-enriched Cl added to total Cl aliquot (µg)[b]	^{35}Cl / ^{37}Cl[b]	Total Cl concentration (µg g^{-1})	Rock sample dissolved (g)	Natural Cl carrier added (µg)[c]	^{36}Cl / Cl	^{36}Cl / Cl uncertainty[d]	^{36}Cl concentration (atoms g^{-1})[e]	^{36}Cl concentration uncertainty (atoms g^{-1})[e]	^{36}Cl age (ka)[f]
Rock Samples																			
19SEAK-01[g]	Boulder	55.2449	−133.4328	391	2.0	2.5	2.8	0.995658	1.2063	75.4	1.110	12.9 ± 0.8	12.0014	358	1.47E−13	3.39E−15	1.03E+05	2.41E+03	13.5 ± 0.3 (1.3)
19SEAK-02[h]	Boulder	55.2461	−133.4327	398	2.5	3	2.8	0.994066	1.0383	76.2	1.014	5.7 ± 0.1	11.5081	435	1.74E−13	5.07E−15	1.27E+05	3.73E+03	16.4 ± 0.5 (1.5)
19SEAK-03[i]	Boulder	55.246	−133.4324	398	2.0	2.5	2.8	0.994066	1.2061	76.5	1.282	24.0 ± 0.8	14.0301	171	2.00E−13	4.34E−15	1.22E+05	2.67E+03	13.1 ± 0.3 (1.3)
19SEAK-06[i]	Boulder	55.2448	−133.4355	398	3.0	2	2.8	0.995524	1.2081	79.5	1.088	9.3 ± 0.6	20.0269	314	2.43E−13	5.09E−15	1.03E+05	2.16E+03	12.4 ± 0.3 (1.1)
Process blanks																			
CLBLK-AQ4	–	–	–	–		–	–	–	–	78.0	0.953		–	–	–	–	–		–
CLBLK-AQ6	–	–	–	–		–	–	–	–	78.0	0.938		–	–	–	–	–		–
CLBLK-AQ8	–	–	–	–		–	–	–	–	76.6	0.936		–	–	–	–	–		–
CLBLK-26	–	–	–	–		–	–	–	–	–	–		–	0.1998	2.37E−15	9.24E−16	–		–

[a] Elevations and positions were recorded with a Garmin handheld GPS receiver (∼ 5 m vertical uncertainty) or GAIA GPS (∼ 5 m vertical uncertainty). [b] The ^{37}Cl-enriched spike was made at Lawrence Livermore National Laboratory. Its Cl concentration is 1285 ppm and its ^{35}Cl / ^{37}Cl ratio is 0.93. [c] The natural Cl carrier was made by dissolving Weeks Island Halite in deionized water at the University of New Hampshire. Its Cl concentration is 1436 ± 9 ppm and its ^{35}Cl / ^{37}Cl ratio is 3.127. [d] Uncertainties on ^{35}Cl / ^{37}Cl and ^{36}Cl / Cl ratios and exposure ages represent propagated 1σ analytical uncertainties only. [e] Sample ^{36}Cl concentrations are corrected for ^{36}Cl contributed by process blank CLBLK-26. [f] Exposure ages are presented at 1σ internal uncertainty; external uncertainty shown in parentheses. Ages were calculated with an online exposure age calculator (http://stoneage.ice-d.org/math/Cl36/v3/v3_Cl36_age_in.html) and Lm scaling (Lal, 1991) assuming no surface erosion and steady-state nucleogenic ^{36}Cl production. [g] Aliquot for stable Cl measurements processed with CLBLK-AQ6. [h] Aliquot for stable Cl measurements processed with CLBLK-AQ8. [i] Aliquot for stable Cl measurements processed with CLBLK-AQ4.

Archipelago) and from a flat bench scattered with boulders on the summit's flank for ^{10}Be dating (Fig. 6). The two boulders sampled on the bench date to 15.6 ± 0.7 (19SEAK-07; Fig. 3) and 15.0 ± 1.1 ka (19SEAK-08; we report all surface exposure ages with 1σ internal uncertainty; Table 1). The summit site featured fresh glacially sculpted bedrock surfaces with a couple boulders resting on the bedrock. A boulder and its adjacent bedrock surface, as a pair, date to 17.4 ± 1.2 (19SEAK-09) and 19.7 ± 1.2 ka (19SEAK-10), respectively (Fig. 3). The three boulders yield a mean age of 16.0 ± 1.2 ka ($n = 3$; 1 SD).

On southwestern Suemez Island, we sampled four large boulders for ^{36}Cl dating. The boulders were distributed across a terrain of patchy muskeg with locally outcropping bedrock. Based on reconstructed Cordilleran Ice Sheet flow directions (Lesnek et al., 2020) and boulder composition (Table S2; Eberlein et al., 1983), the boulders were likely plucked from basalt flows present on the southwestern portion of Suemez Island (Brew, 1995). The four basalt boulders from southwestern Suemez Island have ^{36}Cl exposure ages ranging from 12.4 ± 0.3 to 16.4 ± 0.5 ka (ages are reported at 1σ internal uncertainty; Fig. 5; Table 2). ^{36}Cl surface exposure ages assuming 3 mm kyr^{-1} of surface erosion and non-steady-state nucleogenic ^{36}Cl production are presented in Table S3; for all four samples, changing these parameters results in calculated surface exposure ages < 2 % higher than those presented in the main text.

We collected samples from four sites (Baranof Sites A–D; Fig. 7) on the ocean-facing side of Baranof Island, northern Alexander Archipelago. Here, we chose our helicopter ground stops in an area previously mapped as ice-free throughout the LLGM (Carrara et al., 2007; Fig. 7). Evidence for glacial sculpting of bedrock surfaces is clear; glacial grooves, striations, and chatter marks are present at all sites, and the bedrock surfaces, in places, are topped by perched boulders (Fig. 3). Field evidence of recent glaciation, including relatively unweathered chatter marks, grooves, and striations, contradicts prior mapping of these areas being ice-free during the LLGM.

Baranof Site A is a large, unforested area of bedrock outcrops composed of several smaller ridges. Here, we sampled two bedrock surfaces – one from the stoss side of a bedrock outcrop (19SEAK-18; Fig. 3) and one from the top surface of a nearby bedrock patch (19SEAK-19) – which date to 21.7 ± 0.9 and 28.0 ± 1.1 ka, respectively. A boulder sampled adjacent to bedrock (sample 19SEAK-18) yielded an exposure age of 16.9 ± 0.8 ka (19SEAK-17). A second boulder sample from this site dates to 14.4 ± 0.7 ka (19SEAK-20; Fig. 3). At Baranof Site B – a raised bedrock knob – we sampled two boulders and one bedrock surface. The two boulders have ^{10}Be ages of 15.1 ± 0.6 ka (19SEAK-23; Fig. 3), 14.4 ± 0.7 ka (19SEAK-21); the bedrock sample has a ^{10}Be age of 14.4 ± 0.6 ka (19SEAK-22). Baranof Site C is a high ridge between the ocean and a U-shaped valley with abundant bedrock outcrops and few boulders. Here, a boulder yielded an exposure age of 16.3 ± 0.6 ka (19SEAK-24; Fig. 3), whereas a bedrock surface dates to 15.7 ± 0.6 ka (19SEAK-25). Finally, Baranof Site D is a small bedrock ridge between two peaks with massive stoss and lee features. At this site, we collected samples from two quartz veins in the bedrock, which have exposure ages of 18.2 ± 0.7 (19SEAK-26; Fig. 3) and 20.2 ± 0.8 ka (19SEAK-27). Because the sites are all in relatively close proximity and from similar elevations (50–160 m a.s.l.), we treat the samples as having experienced the same glacial history, and thus should belong to a single age population. Collectively, boulder samples yield a mean age of 15.4 ± 1.1 ka ($n = 5$; 1 SD) with no obvious outliers, whereas the bedrock samples exhibit more scatter and are mostly older than the mean boulder age (Fig. 9).

Biorka Island, a small island off the western coast of central Baranof Island, was initially mapped as ice-covered throughout the LLGM (Dyke, 2004). Here, there are numerous ∼ 1 m tall boulders that rise above the surrounding vegetation and rest on ice-sculpted bedrock. Vegetation and sediments mostly obscure underlying bedrock surfaces, and thus we only collected samples from boulders at this sampling site. Our four boulder samples yielded exposure ages of 15.3 ± 0.5 (18JB005; Fig. 4), 14.9 ± 0.6 (18JB006), 15.4 ± 0.5 (18JB007; Fig. 4), and 13.7 ± 0.5 ka (18JB008), with a mean of 14.8 ± 0.8 ka ($n = 4$; 1 SD; Fig. 8).

We visited a summit ridge at 545–560 m a.s.l. on the western, ocean-facing side of northwestern Kruzof Island, previously mapped as ice-free throughout the LGM (Dalton et al., 2020). There, we found many large stable boulders and exposed patches of glacially sculpted bedrock between vegetation exhibiting glacial grooves and chatter marks. Here, we sampled three large boulders (> 2 × 2 × 1 m), which date to 14.9 ± 0.8 (20SEAK-07; Fig. 4), 14.9 ± 0.9 (20SEAK-12) and 14.6 ± 0.8 ka (20SEAK-13; Fig. 4), yielding a mean age of 14.8 ± 0.2 ka ($n = 3$; 1 SD; Fig. 8). A bedrock surface at this site dates to 13.4 ± 1.0 ka (20SEAK-10; Fig. 4) and sits ∼ 10 m below and ∼ 10 m away from the boulder that dated to 14.6 ± 0.8 ka (20SEAK-13).

We collected samples from three sites on Chichagof Island (Chichagof Sites A–C; Fig. 8). Unlike our other sampling locations which are on the ocean-facing, western sides of the archipelago, the Chichagof Island sites are all located inland. We visited these sites to determine the timing of ice retreat inland and to complement the findings of a previous study that documented ice withdrawal in the central and eastern Alexander Archipelago (Lesnek et al., 2020). Chichagof Island is notable for its relative lack of boulders – consequently, the boulders sampled here are smaller than those at other sites. While many bedrock outcrops featured smooth surfaces indicative of glacial erosion, we did not observe clear striations or chatter marks. At site A, a bedrock bench, ^{10}Be ages from two small, perched boulders are 12.7 ± 0.7 (20SEAK-15; 0.5 × 0.3 × 0.3 m; 476 m a.s.l.; Fig. 4) and 9.0 ± 0.6 ka (20SEAK-16; 0.5 × 0.4 × 0.3 m; 473 m a.s.l.). A

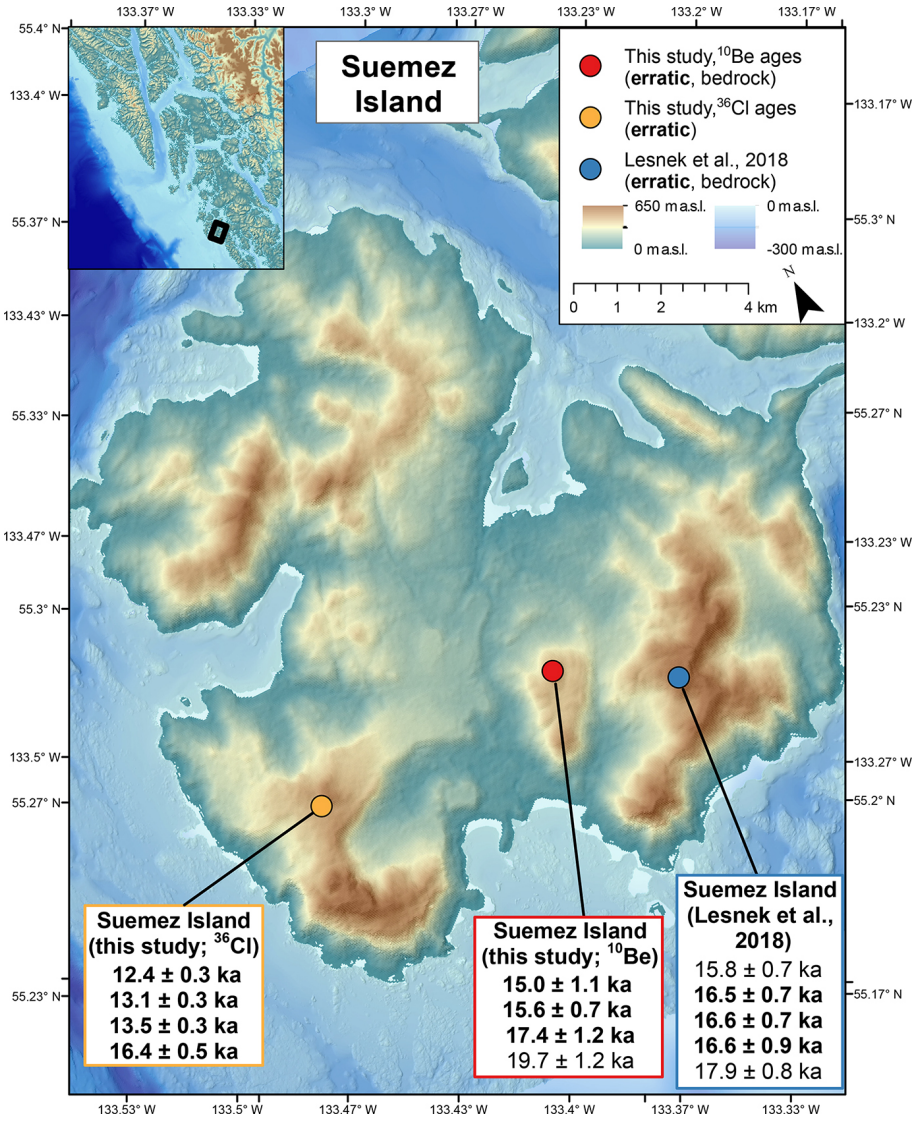

Figure 6. ^{10}Be and ^{36}Cl ages from samples collected on Suemez Island: red and yellow dots mark sampling site from this study, blue dot marks sampling site from Lesnek et al. (2018). Bold ages are from boulders; plain ages are from bedrock. All ^{10}Be and ^{36}Cl ages reported with 1σ internal uncertainty.

quartz vein sampled from bedrock outcrop at this site has an exposure age of 15.3 ± 0.7 ka (20SEAK-14). Site B is a series of bedrock ridges, and a single boulder yields an exposure age of 12.4 ± 0.9 ka (20SEAK-18; 817 m a.s.l.; Fig. 4), while an adjacent bedrock surface dates to 14.1 ± 0.7 ka (20SEAK-19; 816 m a.s.l.). Finally, site C is at the summit of a massif and one bedrock knob sampled here has an exposure age of 17.7 ± 0.8 ka (20SEAK-22; 779 m a.s.l.; Fig. 4).

5 Discussion

5.1 Bedrock ^{10}Be ages

We sampled large and stable boulders in addition to bedrock surfaces with clear evidence of glacial erosion (e.g., striations, chatter marks) with the goal of providing optimal constraints on deglaciation. Sampling bedrock surfaces also allows us to better understand the subglacial erosion regime across the Alexander Archipelago, potentially yielding information about the duration of ice cover, the amount of subglacial erosion, and the likelihood of boulders containing inheritance.

Bedrock exposure ages are older than the mean boulder exposure ages by 2 SD or greater on Suemez Island (19SEAK-10) and Baranof sites A (19SEAK-18, 19SEAK-19) and D (19SEAK26, 19SEAK-27). At Chichagof site A the bedrock exposure age (20SEAK-14) is ~ 4.5 kyr older than the mean boulder age but still within 2 SD, perhaps due to the large spread in boulder ages resulting in larger standard deviations.

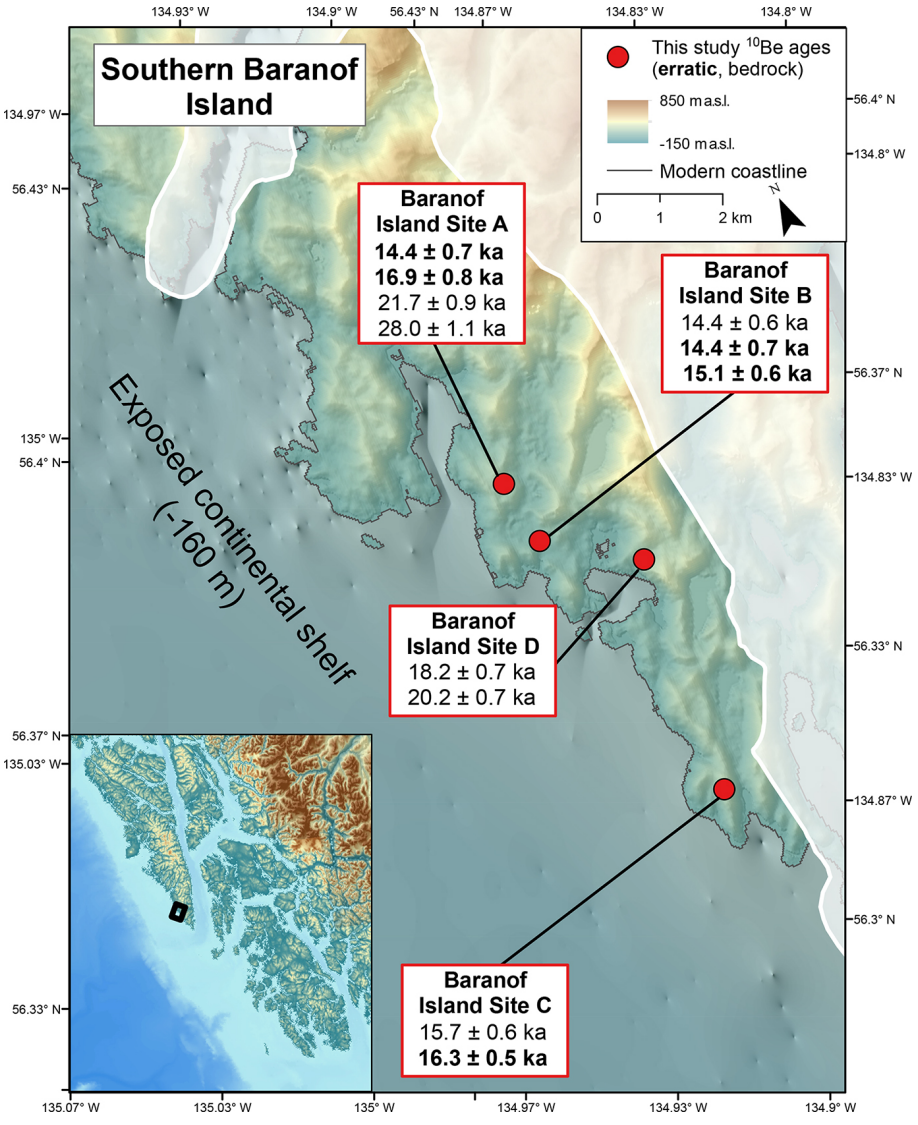

Figure 7. ^{10}Be ages from sampling sites on southern Baranof Island. Bold ages are from boulders; plain ages are from bedrock. All ages are reported with 1σ internal error. Cordilleran Ice Sheet LLGM extent after Carrara et al. (2007).

At Chichagof site B, the single boulder ^{10}Be age (20SEAK-18) post-dates the single bedrock age by ∼ 1.7 kyr. In general, bedrock data reported here are consistent with bedrock ^{10}Be ages from Warren and Baker islands that are older (by more than 2 SD) than mean boulder ages (Lesnek et al., 2018). Bedrock ages may be erroneously older due to ^{10}Be inheritance if ice sheet erosion was insufficient to remove the ∼ 2 m of rock required to remove most of the previous ^{10}Be inventory. Studies from British Columbia (Darvill et al., 2018) and Washington (Briner and Swanson, 1998) also report cosmogenic nuclide inheritance in bedrock from other areas covered by the Cordilleran Ice Sheet. In our field area, the short-lived nature of the overriding event (∼ 3 kyr; Lesnek et al., 2018) may also contribute to the lack of significant glacial erosion. Finally, traces of inheritance may be present in bedrock, perhaps even boulders, in ice-sheet-distal sites like these that are overrun by ice during extremely brief portions of the Quaternary (Briner et al., 2016).

In some cases, boulder–bedrock pairs have similar exposure ages (on southern Baranof and Suemez islands), suggesting our bedrock ages are unaffected by ^{10}Be inheritance at these sites. On Kruzof Island, a bedrock patch yields an exposure age that is younger (by more than 2σ) than the mean age of the surrounding boulders. Potential cover by snow, sediment, or vegetation is thought to have caused anomalously young ages elsewhere in the Alexander Archipelago (Lesnek et al., 2020) and may also explain this ^{10}Be age from our bedrock site on Kruzof Island.

Bedrock exposure ages vary greatly (by as much as ∼ 14 kyr) between the various sampling locations on Bara-

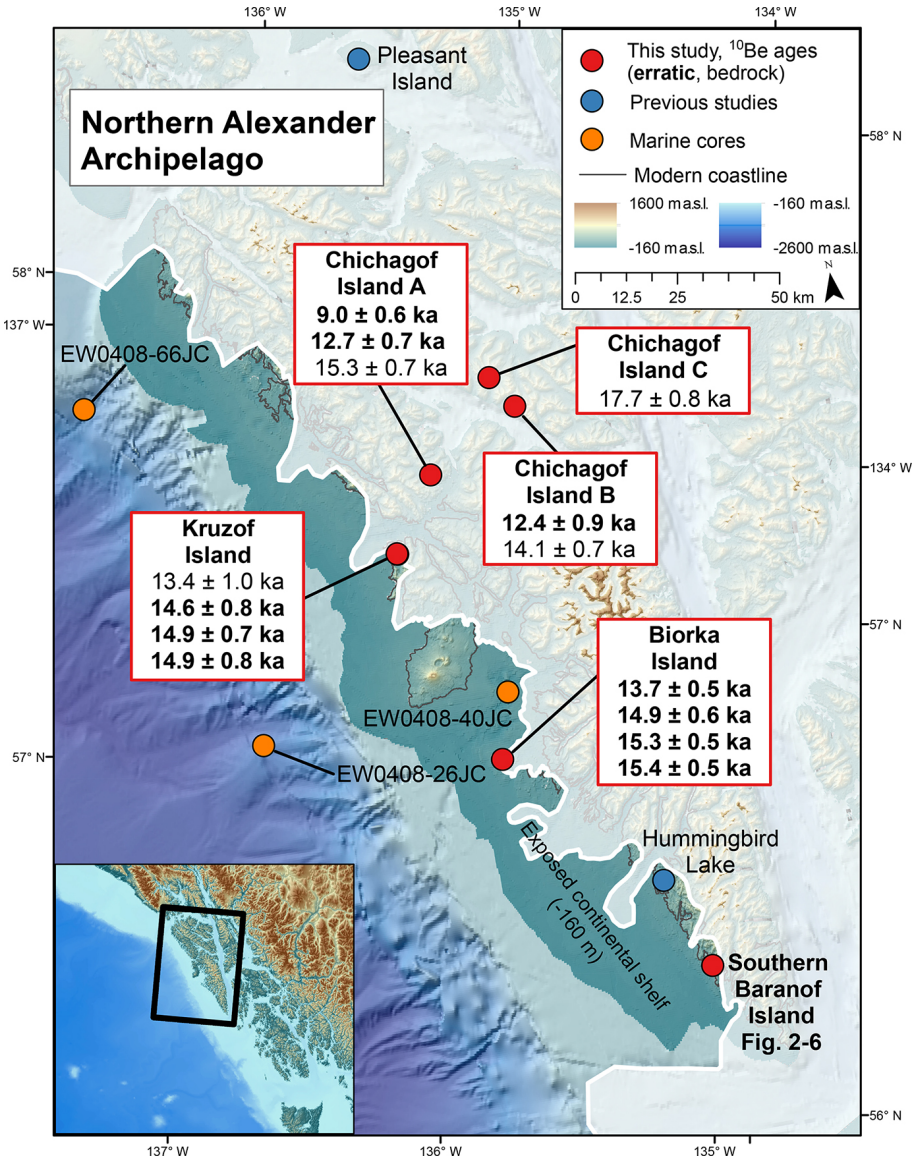

Figure 8. ^{10}Be ages from sampling sites in the northern Alexander Archipelago. All ages are reported with 1σ internal error. Bold ages are from boulders; plain ages are from bedrock. LLGM Cordilleran Ice Sheet extent after Lesnek et al. (2020). Exposed continental shelf at −160 m below modern sea level Baichtal et al. (2021). Yellow dots show location of relevant marine sediment cores: EW0408-66JC and EW0408-26JC (Praetorius and Mix, 2014; Praetorius et al., 2016) and EW0408-40JC (Addison et al., 2010). Blue dots show locations of relevant terrestrial study sites: Pleasant Island (Hansen and Engstrom, 1996) and Hummingbird Lake (Ager, 2019).

nof Island and up to 6 kyr on Suemez Island (Lesnek et al., 2018). The Alexander Archipelago is characterized by impressive relief (deep fjords, high peaks), and thus, sub-glacial erosion rates clearly varied greatly across Suemez and Baranof islands where sampling locations are ∼2–6 km apart. Differing bedrock ^{10}Be ages from the same sampling locales confirm this inference, reflecting variable sub-glacial erosion rates even within ∼100 m of each other. Some samples may have been collected in areas dominated by glacial abrasion, whereas other samples might be from surfaces dominated by quarrying, and thus, this variability could reflect varying sub-glacial processes on a local scale.

Because bedrock exposure ages from the coastal Alexander Archipelago (this study; Lesnek et al., 2018) do not consistently pre-date, match, or post-date exposure ages from adjacent boulders, we refrain from including bedrock-based ^{10}Be ages in our mean deglaciation age calculations (Figs. 9, 10). This negates biases when choosing which bedrock ages "match" nearby erratic ages and allows us to eliminate any concern over inheritance or post-ice retreat cover of these bedrock surfaces. While bedrock ages, especially when

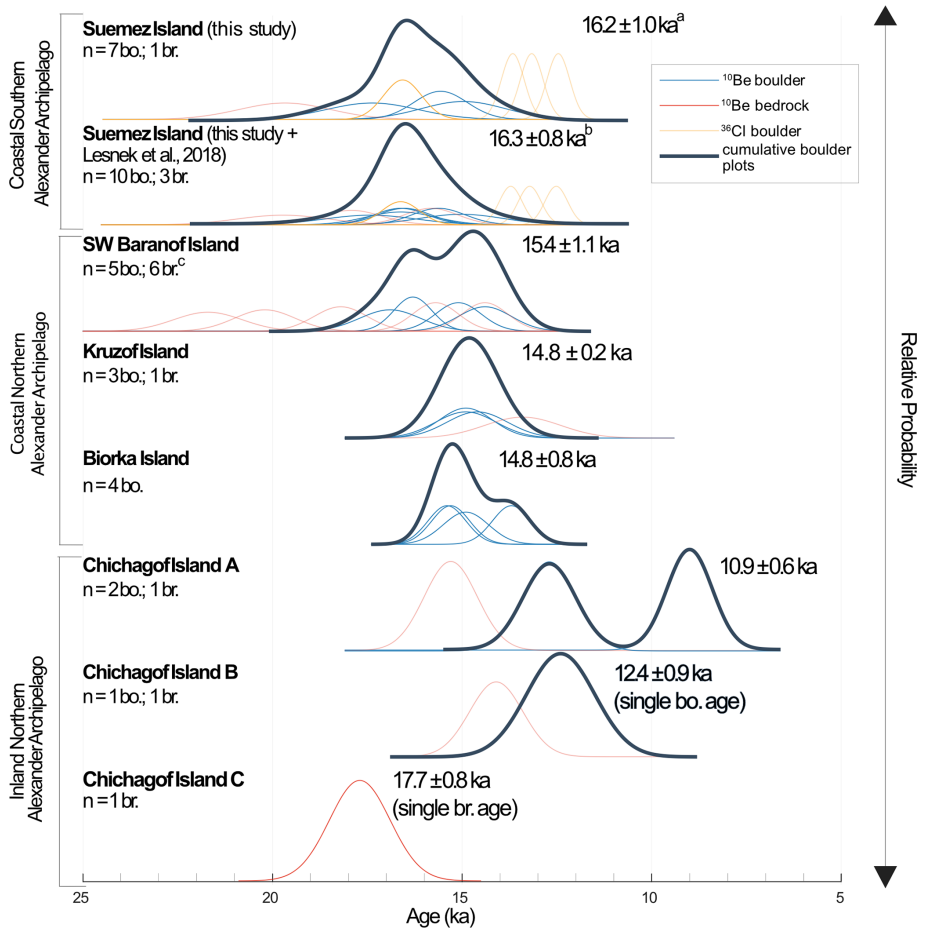

Figure 9. Relative probably plots of bedrock (red) and boulder (blue) ^{10}Be and ^{36}Cl boulder (yellow) ages from this study calculated with 1σ internal uncertainty. bo. – boulder, br. – bedrock. All ages shown are mean ages from only boulders at each sample site reported with 1 SD unless noted. Cumulative plots represent all bold lines – transparent lines were not included in their calculation. [a] Average of all ^{10}Be boulder ages and oldest ^{36}Cl boulder age with 1 SD. [b] Average of all ^{10}Be boulder ages (this study and Lesnek et al., 2018) and oldest ^{36}Cl boulder age (this study). [c] One old outlier at 28.0 ± 1.1 ka not shown.

paired with boulder ages, are useful for identifying spatially variable subglacial erosion processes and issues with past cover and inheritance, they do not appear to provide reliable age constraints on the timing of deglaciation in the Alexander Archipelago due to the inconsistencies between bedrock and boulder ages. In light of this, we also recalculate relevant mean ages from Lesnek et al. (2018, 2020) using solely boulder ^{10}Be ages to update these other regional chronologies.

5.2 ^{10}Be chronology incompatible with mapped Cordilleran Ice Sheet extent

We targeted areas of the northern Alexander Archipelago mapped as ice-free by previous studies to determine whether these areas were LLGM refugia. The most recent coastal Cordilleran Ice Sheet reconstructions show significant portions of the northern Alexander Archipelago as remaining ice-free throughout the LLGM (Fig. 2), with ice terminating close to the present shoreline – not on the continental shelf (Dalton et al., 2020; Lesnek et al., 2020). Our data, however, indicate that at least some of these areas previously mapped as refugia (southwestern Baranof and Kruzof islands) were covered by ice, and deglaciated around 15.4–14.8 ka. Our new evidence thus suggests that ice extended onto the continental shelf during the LLGM, as in the southern Alexander Archipelago (Lesnek et al., 2018). These discrepancies between previously mapped ice extents and those implied by our new exposure ages highlight the need to develop deglaciation chronologies elsewhere along the Cordilleran Ice Sheet coastal margin to provide updated mapping around the North Pacific.

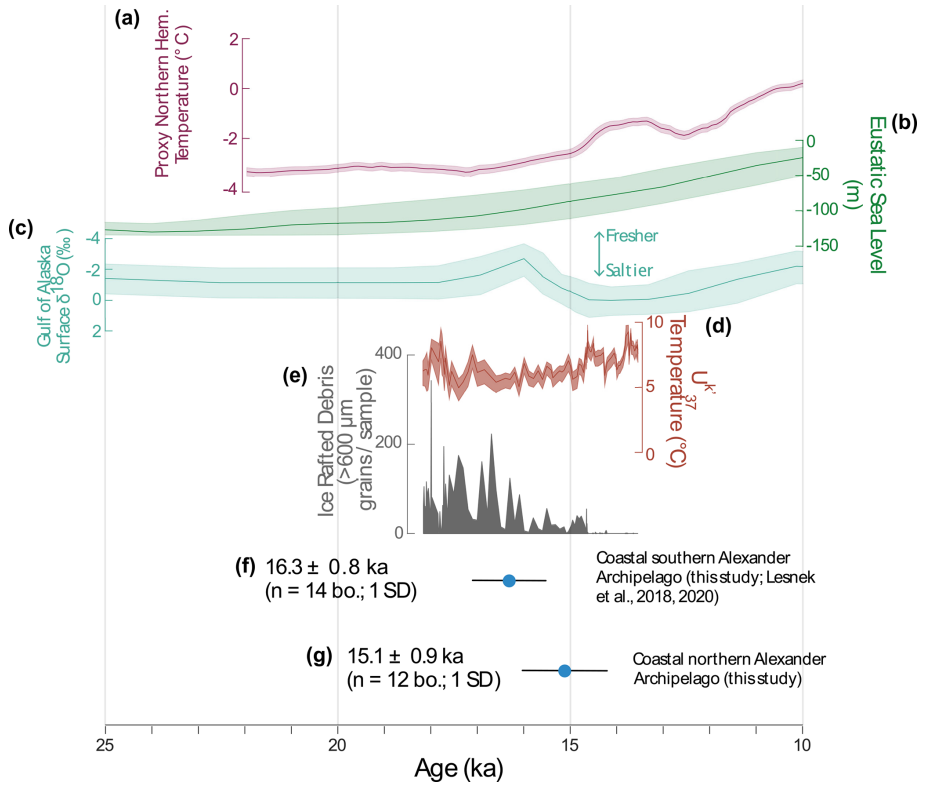

Figure 10. **(a)** Proxy northern hemispheric temperature anomaly relative to early Holocene with 1σ error (Shakun et al., 2012). **(b)** Eustatic sea-level curve (Spratt and Lisiecki, 2016). **(c)** Gulf of Alaska surface salinity $\delta^{18}O$ record (Core SO202-27-6; Maier et al., 2018). **(d)** $U^{k'}_{37}$ temperature reconstruction from off the coast of the Alexander Archipelago (Cores EW0408-26JC, EW0408-66JC; Praetorius et al., 2016). **(e)** Ice-rafted debris record from off Vancouver Island (Core MD02-2496; Cosma et al., 2008). **(f, g)** Mean boulder ^{10}Be ages from the coastal Alexander Archipelago, with 1σ r (this study; Lesnek et al., 2018, 2020).

5.3 Cordilleran Ice Sheet retreat across the Alexander Archipelago

Mean boulder ^{10}Be exposure ages from Suemez Island in this study and Lesnek et al. (2018), $16. \pm 1.2$ ka ($n = 3$ boulders; 1 SD) and 16.6 ± 0.8 ka ($n = 3$ boulders; 1 SD), respectively, overlap within 1 SD (Figs. 6, 9). However, three of the boulder ^{36}Cl ages from southwestern Suemez Island do not overlap with the ^{10}Be ages at 1 SD (Figs. 6, 9). We attribute this scatter to post-depositional surface erosion of the basaltic boulders (i.e., those dated with ^{36}Cl) in excess of 3 mm kyr^{-1}. Although we targeted areas of the boulder tops with no obvious signs of erosion, given the maritime climate of southeastern Alaska it is possible that the original, glacially eroded boulder surfaces have been weathered. Surface erosion of rocks with low concentrations of native Cl (Table S2), where the primary ^{36}Cl production pathway is Ca spallation (Marrero et al., 2016), results in exposure ages that are erroneously young. Thus, we interpret the oldest ^{36}Cl exposure age (16.4 ± 0.5 ka; 19SEAK-02) as the closest constraint on deglaciation at that site. This ^{36}Cl age overlaps with the ^{10}Be ages from elsewhere on Suemez Island; we combine them and calculate a new, boulder-based mean deglaciation age of 16.3 ± 0.8 ka ($n = 10$ boulders; 1 SD) for Suemez Island.

We group together three of our sampling locations in the northern Alexander Archipelago that are ocean-facing: Kruzof, Biorka, and southern Baranof islands. As the Cordilleran Ice Sheet retreated from the continental shelf inland, these were the first areas presently above sea level to become ice-free. We calculate a mean ^{10}Be boulder age of 15.1 ± 0.9 ka ($n = 12$ boulders; 1 SD) for the coastal northern Alexander Archipelago.

There are limited data from elsewhere in the northern Alexander Archipelago that constrain the timing of deglaciation. A basal pollen concentrate-based radiocarbon age from Hummingbird Lake (Fig. 7), southwestern Baranof Island, dates to 15.0 ± 0.2 cal ka, in agreement with the ^{10}Be ages presented here and that collectively indicate coastal Baranof Island was deglaciated prior to ~ 15 ka (Ager, 2019). Additionally, tephra layers from Mt. Edgecumbe on Kruzof Island are dated to 13.1 ka (Riehle et al., 1992; Begét and Motyka, 1998) and blanket many of the surrounding islands, suggesting that these areas were ice-free by then.

All three sample sites on Chichagof Island (Sites A–C) are not ocean-adjacent and characterized by a general

lack of boulders. The boulders present were much smaller and shorter (< 0.5 m high) than boulders sampled elsewhere across the Alexander Archipelago – we chose to sample these despite their size to provide minimum ages for deglaciation and to compare with available radiocarbon constraints. The ages of these boulders fall between 9.0 ± 0.6 and 12.7 ± 0.7 ka and are thus younger than other age constraints for deglaciation on Chichagof Island; radiocarbon ages on shells from raised marine terraces on Chichagof Island date back to 14.2 ± 0.6 cal ka suggesting that the island was ice-free by this time (Baichtal et al., 2021). Smaller boulders are more susceptible to cover (whether snow, vegetation, or sediment) and may thus yield anomalously young ^{10}Be ages. While a lack of large boulders found on Chichagof Island makes it difficult to ascertain the timing of deglaciation, regional glacial and sea-level history suggests Chichagof Island was deglaciated between 15.1 ka (when the coastal area deglaciated) and 14.2 cal ka (the age of shells in raised marine deposits). Therefore, the boulders dated here likely have anomalously young exposure ages.

Our mean ^{10}Be age of 15.1 ± 0.9 ka ($n = 12$ boulders; 1 SD) from all sites along the coastal portion of the northern Alexander Archipelago fits with the few other regional deglaciation constraints (Fig. 2) and overlaps within 1 SD with the mean boulder exposure age from the southern Alexander Archipelago of 16.3 ± 0.8 ka ($n = 13$ boulders; 1σ; this study; Lesnek et al., 2018, 2020). While mean ages from the northern and southern Alexander Archipelago overlap within 1 SD, it is possible that these areas deglaciated at slightly different times as these various sampling sites happened to become ice-free. Furthermore, local ice caps formed and radiated from massifs on Chichagof, Baranof, and Prince of Wales islands during the LLGM (Capps, 1932; Mann and Hamilton, 1995; Lesnek et al., 2020). These local ice caps served as a local ice source for the Alexander Archipelago, and their locations and flow patterns may have led to some parts of the archipelago becoming ice-free before others. Thus, we present a range of deglaciation across the coastal Alexander Archipelago from between 16.3 ± 0.8 and 15.1 ± 0.9 ka.

Ice retreat across the Alexander Archipelago is also registered in marine sediments off the former coastal Cordilleran Ice Sheet margin. Several marine sedimentary records (cores EW0408-26JC, EW0408-66JC, EW0408-85JC) extending back to ∼ 18.5 cal ka show the presence of ice-rafted debris (IRD) beginning ∼ 18.5 ka, peaking at 17.5–16.5 ka, and ceasing at 14.8 ka, reflecting a final retreat of marine-terminating ice (Praetorius and Mix, 2014). Furthermore, these IRD data record fluctuating but relatively elevated calving spanning 18.5 to 14.8 ka, perhaps indicating steady retreat punctuated by periods of accelerated melting.

Tephra from Mt. Edgecumbe (Kruzof Island) found in core EW0408-26JC is interpreted to have been deposited in a submarine environment, suggesting that this core site was ice-free by 14.6 ka (Praetorius et al., 2016). Records of a subsequent eruption dated to ∼ 13.1 cal ka from marine sediments in Sitka Sound (core EW0408-40JC) indicate that this area (between Baranof and Kruzof islands) must have been ice-free by this time (Addison et al., 2010). Finally, ^{14}C ages from mollusks found in a diamicton layer along the Gastineau Channel date to ∼ 13.8 cal ka, reflecting the beginning of deglaciation near the mainland (Miller, 1973; we calibrate all uncalibrated ^{14}C ages with CALIB 8.2; http://calib.org/calib/, last access: 14 March 2022).

5.4 Chronologies of Cordilleran Ice Sheet deglaciation across the North Pacific

Radiocarbon ages from the Cordilleran Ice Sheet margin reflect ice advance from ∼ 20–17 ka, near the end of the GLGM at 19 ka. Ages from mammalian fossils in Shuká Káa on Prince of Wales Island indicate Cordilleran Ice Sheet advance ∼ 20 ka in the Alexander Archipelago (Lesnek et al., 2018). Directly south of the Alexander Archipelago, on eastern Graham Island (Haida Gwaii) initial ice advance is dated to 24.1–22.5 cal ka with a ^{14}C date from a twig underlying till (Blaise et al., 1990; Mathewes and Clague, 2017). Along the southwestern Cordilleran Ice Sheet margin, ice reached its maximum extent until ∼ 17.0 ka in the Puget Sound area (Porter and Swanson, 1998).

Glacier chronologies from the northeastern Pacific coastline also reflect post-GLGM retreat. On Sanak Island, tephra near the bottom of a lake sediment core dates deglaciation before ∼ 15.9 ka, broadly synchronous with Cordilleran Ice Sheet withdrawal in the Alexander Archipelago (Misarti et al., 2012). On Kodiak Island, final LLGM retreat dates to ∼ 15.7 cal ka, as marked by a ^{14}C age above glaciotectonically altered sediments (Mann and Peteet, 1994). Directly north of the Alexander Archipelago, a ^{14}C age from a log found within the Finger Glacier lateral moraine provides a minimum age of deglaciation at ∼ 14.6 cal ka (Mann, 1986). Radiocarbon ages from a marine sediment core in Dixon Entrance date maximum Cordilleran Ice Sheet extent to before ∼ 16.1 cal ka and retreat beginning before ∼ 15.3 cal ka (Barrie and Conway, 1999). A marine sediment record from Vancouver Sound similarly dates maximum ice extent to 18.5 ka and retreat of the Cordilleran Ice Sheet onto the mainland by 16.4 ka (Blaise et al., 1990). Quaternary sediments on eastern Graham Island indicate the Cordilleran Ice Sheet was retreating by 17.8 cal ka (Blaise et al., 1990). Notably, ^{10}Be ages on Calvert Island suggest ice retreated off the continental shelf at ∼ 18 ka, pre-dating ice withdrawal onto land in the Alexander Archipelago (Darvill et al., 2018).

Marine sediment cores are interpreted to show ice retreat across the coastal northeastern Pacific. A marine sediment core (SO202-27-6) from the Gulf of Alaska captures a decrease in sea surface salinity ∼ 16 ka, interpreted to reflect increased meltwater from the Cordilleran Ice Sheet margin (Maier et al., 2018). Another marine sediment core (EW0408-85JC) recovered off the coast of southern Alaska

records a decrease in glacial-margin sediment accumulation at 16.9 ka as ice stagnated or began to retreat (Davies et al., 2011). Reductions in salinity captured by planktonic δ^{18}O in this core at ∼ 16.7 ka are interpreted as an increase in meltwater input from retreating glaciers. A transition from ice-proximal to laminated hemipelagic sediments at ∼ 14.8 ka marks glacier retreat off the continental shelf and onto land. Off the coast of Alaska, a marine sediment core records a peak of IRD deposition between 18 and 17 ka, interpreted as the retreat of marine-terminating margins of the Cordilleran Ice Sheet (Walczak et al., 2020). Additionally, another core from off Vancouver Island (MD02-2496) captures IRD deposition between ∼ 17.0 and ∼ 16.2 cal ka – indicating rapid regional deglaciation – and a minor IRD event at ∼ 14.7 cal ka (Cosma et al., 2008).

Our new data showing ice retreat at 15.1 ± 0.9 ka from the northern Alexander Archipelago, along with ages of deglaciation from the southern Alexander Archipelago (16.3 ± 0.8 ka; this study; Lesnek et al., 2018), are broadly synchronous with previously published ice retreat chronologies for the marine-terminating Cordilleran Ice Sheet margin elsewhere along the northeastern Pacific Coast. However, while our chronology only documents deglaciation, it provides further evidence of a delayed LLGM across the coastal Cordilleran Ice Sheet compared to the GLGM maximum extents of alpine glaciers in mainland Alaska (Briner et al., 2017), parts of southern Alaska (Reger et al., 1996), and the Laurentide Ice Sheet (Dalton et al., 2020).

5.5 Paleoclimate records from the North Pacific

Several paleoclimate records from around the North Pacific span our interval of Cordilleran Ice Sheet deglaciation in the Alexander Archipelago. A combined diatom assemblage- and alkenone-derived record of sea surface temperatures (SSTs) from the Bering Sea (Core 51JPC) records perennial sea ice from ∼ 22.5 ka (beginning of record) to 17 ka and increased SSTs beginning ∼ 16.9 ka before a notable shift back to annual sea ice ∼ 16.7 ka (Caissie et al., 2010). In the northern Gulf of Alaska (Core EW0408-85JC), δ^{18}O data document increasing SSTs at 16.7 ka and again at ∼ 14.7 ka (Davies et al., 2011). Alkenone-inferred paleo-SST reconstructions from this same core show the lowest SSTs (∼ 5 °C) circa 17.0 ka, with increased SSTs beginning ∼ 16.5 ka, and a rapid ∼ 3–4 °C rise in SSTs from 15.2 to 14.7 ka (Praetorius et al., 2015). Alkenone-inferred SST and δ^{18}O records from the Gulf of Alaska also record increased SSTs of ∼ 3 °C at 14.7 ka (cores EW0408-26JC, EW0408-66JC; Praetorius et al., 2016). Off Vancouver Island, Mg / Ca temperature reconstructions from subsurface-dwelling *N. pachyderma* indicate two stages of warming of ∼ 2 °C at 17.2–16 ka, and a further ∼ 3 °C 15.5–14.0 ka, while surface-dwelling *G. bulloides* record a 3 °C SST increase from 15.0–14.0 ka (core MD02-2496; Taylor et al., 2014), all within the uncertainty of coastal Alexander Archipelago ice retreat. Alkenone SST reconstructions from another nearby core (core JT96-09) also indicate a 4 °C increase in SST at ∼ 14.7 ka (Kienast and McKay, 2001).

There are few terrestrial paleoclimate data that span the last deglacial period from southeastern Alaska and coastal British Columbia. Cordilleran ice cover until ∼ 15 ka across much of the region impeded the preservation of many terrestrial records – however, there are limited ice core, speleothem, and lake records that date back to early regional deglaciation or prior. A growth hiatus in a speleothem from El Capitan Cave (southern Alexander Archipelago) spanning ∼ 41.5 to ∼ 13.4 ka suggests the cave was either overridden by the Cordilleran Ice Sheet, experienced permafrost conditions and a mean annual air temperature < 0 °C, or lacked drip water (Wilcox et al., 2019). The youngest date also serves as a minimum limit on deglaciation, as the area was thawed by ∼ 13.4 ka. However, El Capitan Cave is ∼ 60 km inland of the outermost coastal region and therefore may have still experienced these conditions while the outer coast deglaciated. At Hummingbird Lake, southwestern Baranof Island, pollen records indicate *Pinus contorta* dominated from ∼ 15.2 to 14 ka, which is interpreted to represent *Pinus contorta* response to the beginnings of Gulf of Alaska ocean warming at ∼ 16.5 ka (Praetorius et al., 2015; Ager, 2019). This record suggests increased air temperatures around deglaciation of the Alexander Archipelago between 16.3 ± 0.8 and 15.1 ± 0.9 ka.

5.6 Implications for early human migration

Several studies have scrutinized potential areas of LLGM glacial refugia in the Alexander Archipelago through a human migration perspective (Carrara et al., 2007; Lesnek et al., 2018), building off similar approaches from elsewhere in the North Pacific (e.g., Warner et al., 1982; Mann and Peteet, 1994; Misarti et al., 2012). Our study focused on southern Baranof and Kruzof islands because previous mapping suggested that parts of these areas were ice-free throughout the LLGM (Carrara et al., 2003, 2007). However, our ^{10}Be ages from southern Baranof Island indicate these areas were glaciated throughout the LLGM and not available for human habitation between ∼ 20 and ∼ 15.4 ka. Our exposure ages from Kruzof Island also suggest this area was not ice-free until ∼ 14.8 ka.

These results indicate that some of the last major unevaluated areas of possible refugia presently above sea level were covered by ice during the LLGM. At its maximum extent, ice likely extended onto the then-exposed continental shelf. Ice occupation of the continental shelf – or at least parts of the shelf – off the Alexander Archipelago was relatively brief, from ∼ 20.0 to ∼ 16.0 ka (Lesnek et al., 2018). Areas of the continental shelf would have been above modern sea level during this time and until ∼ 11–8 ka, when sea level neared modern levels in the Alexander Archipelago (Baichtal et al., 2021). At a minimum, ice lobes would have existed within

the major shelf troughs (e.g., Chatham Strait), likely crossing the entire shelf at these locations; at a maximum, the entire continental shelf may have been occupied by ice from ∼ 20 to ∼ 16 ka. Whether portions of the shelf remained ice-free during the LLGM is unknown, but it is possible. Based on the immediate colonization of *Pinus* at 15.2 ka in Hummingbird Lake and as early as ∼ 15.4 ka on Pleasant Island, there were likely ice-free areas on the shelf throughout the LLGM (Hansen and Engstrom, 1996; Ager, 2019).

6 Conclusions

We conclude that several areas in southeastern Alaska previously mapped as ice-free through the LLGM were covered by ice until between ∼ 16.3 and ∼ 15.1 ka. ^{10}Be ages from boulders suggest that the northern coastal Alexander Archipelago deglaciated at 15.1 ± 0.9 ka, while ^{10}Be and ^{36}Cl ages date ice retreat in the southern portion at 16.3 ± 0.8 ka, following a LLGM that began after ∼ 20 ka (Lesnek et al., 2018, 2020). The timing of deglaciation in the Alexander Archipelago is similar to some other sites around the Cordilleran Ice Sheet coastal margin (e.g., Mann and Peteet, 1994; Misarti et al., 2012) but later than other locations (e.g., Darvill et al., 2018). Notably, the deglaciation in southeastern Alaska is later than in mainland Alaska and Kodiak and Sanak Islands, Alaska (Fig. 1), where records are more aligned with the GLGM. The timing of deglaciation in the Alexander Archipelago is broadly synchronous with regional records of local ocean and air temperature increases. We also found that anomalously old ^{10}Be ages of bedrock surfaces are likely due to inheritance caused by insufficient ice sheet erosion and thus urge caution when using ages from bedrock surfaces as direct constraints on ice retreat without additional boulder ages along the coastal margins of the Cordilleran Ice Sheet.

Our data indicate that previous mapping of the coastal Cordilleran Ice Sheet can be spatially and temporally improved. We suggest that ice likely extended out on the continental shelf along the Alexander Archipelago. We are increasingly confident that areas of the coastal Cordilleran Ice Sheet previously mapped as ice-free throughout the LLGM were in fact covered by ice, and that refugia, if any existed, would have been located on the exposed continental shelf. Although more logistically challenging, subsequent studies should evaluate the existence of LLGM refugia in the Alexander Archipelago by focusing on the previously exposed continental shelf. Special attention should be given to the northern Alexander Archipelago where ice masses were fed by local ice caps and thus may not have been as extensive, as opposed to elsewhere in the northeastern Pacific where ice was sourced from the main body of the Cordilleran Ice Sheet.

Data availability. Data needed to calculate new exposure ages from this study are found in Tables 1 and 2. Exposure age data included in our mean calculations are from Lesnek et al. (2018, 2020) and will be uploaded to an online cosmogenic exposure age database (ICE-D Alpine; http://alpine.ice-d.org/, last access: 5 April 2022; Balco, 2020).

Supplement. The supplement related to this article is available online at: https://doi.org/10.5194/gchron-4-191-2022-supplement.

Author contributions. JPB designed the study framework and acquired the majority of grant funds. CKW acquired supplementary funding for fieldwork and lab analyses. CKW, JPB, JFB, and AJL collected samples in the field. CKW conducted ^{10}Be work and AJL and JML performed ^{36}Cl chemistry. CKW, JPB, AJL, and JML analyzed sample data and calculated ages. All authors were involved in interpreting the data. CKW wrote the first draft of the manuscript; all authors provided substantial input. CKW and AJL created figures and tables.

Competing interests. The contact author has declared that neither they nor their co-authors have any competing interests.

Disclaimer. Publisher's note: Copernicus Publications remains neutral with regard to jurisdictional claims in published maps and institutional affiliations.

Acknowledgements. We acknowledge that these samples were collected on the ancestral lands of the Tlingit and that the University at Buffalo exists on the land of the Seneca. These peoples are the traditional caretakers of these lands, and we give thanks for the opportunity to exist and work on lands that are rightfully theirs. We thank the Tongass National Forest for assistance with permitting and logistics. We thank Corey Krabbenhoft, Joseph Tulenko, and Karlee Prince for field assistance and Joseph Tulenko and Chris Sbarra for lab assistance. We also thank PRIME Lab for ^{10}Be measurements and Lawrence Livermore National Laboratory for ^{36}Cl measurements. This research was funded by NSF (award no. 1854550), the National Geographic Society (award no. 57989R-19), a Geological Society of America Student Research Grant (grant number 13631) funded by NSF (award no. 1949901), the Alaska Geological Society, and the Mark Diamond Research Fund of the Graduate Student Association at the University at Buffalo, the State University of New York.

Financial support. This research has been supported by the National Geographic Society (grant no. 57989R-19), the Geological Society of America (grant no. 13631), the National Science Foundation (grant no. 1854550), Alaska Geological Society, and the Mark Diamond Research Fund of the Graduate Student Association at the University at Buffalo, the State University of New York.

Review statement. This paper was edited by Yeong Bae Seong and reviewed by Brent Ward and M. Akif Sarikaya.

References

Addison, J. A., Beget, J. E., Ager, T. A., and Finney, B. P.: Marine tephrochronology of the Mt. Edgecumbe volcanic field, southeast Alaska, USA, Quaternary Res., 73, 277–292, https://doi.org/10.1016/j.yqres.2009.10.007, 2010.

Ager, T. A.: Late Quaternary vegetation development following deglaciation of northwestern Alexander Archipelago, Alaska, Front. Earth Sci., 7, 104, https://doi.org/10.3389/feart.2019.00104, 2019.

Baichtal, J. F., Lesnek, A. J., Carlson, R. J., Schmuck, N., Smith, J. L., Landwehr, D. J., and Briner, J. P.: Late Pleistocene and Early Holocene Sea level History Glacial Retreat Interpreted from Shell-bearing Marine Deposits of Southeastern Alaska, Geosphere, 17, 1590–1615, https://doi.org/10.1130/GES02359.1, 2021.

Balco, G.: Production rate calculations for cosmic-ray-muon-produced ^{10}Be and ^{26}Al benchmarked against geological calibration data, Quat. Geochronol., 39, 150–173, 2017.

Balco, G.: Technical note: A prototype transparent-middle-layer data management and analysis infrastructure for cosmogenic-nuclide exposure dating, Geochronology, 2, 169–175, https://doi.org/10.5194/gchron-2-169-2020, 2020.

Balco, G., Stone, J. O., Lifton, N. A., and Dunai, T. J.: A complete and easily accessible means of calculating surface exposure ages or erosion rates from ^{10}Be and ^{26}Al measurements, Quat. Geochronol., 3, 174–195, https://doi.org/10.1016/j.quageo.2007.12.001, 2008.

Barrie, J. V. and Conway, K. W.: Late Quaternary glaciation and postglacial stratigraphy of the northern Pacific margin of Canada, Quaternary Res., 51, 113–123, 1999.

Begét, J. E. and Motyka, R. J.: New dates on late Pleistocene dacitic tephra from the Mount Edgecumbe volcanic field, southeastern Alaska, Quaternary Res., 49, 123–125, 1998.

Blaise, B., Clague, J. J., and Mathewes, R. W.: Time of maximum Late Wisconsin glaciation, West Coast of Canada, Quaternary Res., 34, 282–295, https://doi.org/10.1016/0033-5894(90)90041-I, 1990.

Booth, D. B., Troost, K. G., Clague, J. J., and Waitt, R. B.: The Cordilleran ice sheet, Developments in Quaternary Sciences, 1, 17–43, 2003.

Borchers, B., Marrero, S., Balco, G., Caffee, M., Goehring, B., Lifton, N., Nishiizumi, K., Phillips, F., Schaefer, J., and Stone, J. J. Q. G.: Geological calibration of spallation production rates in the CRONUS-Earth project, Quat. Geochronol., 31, 188–198, 2016.

Brew, D. A.: Geologic map of the Craig, Dixon Entrance, and parts of the Ketchikan and Prince Rupert quadrangles, Southeastern Alaska, No. 95-215, https://doi.org/10.3133/ofr95215, 1995.

Briner, J. P. and Swanson, T. W.: Using inherited cosmogenic ^{36}Cl to constrain glacial erosion rates of the Cordilleran ice sheet, Geology, 26, 3–6, 1998.

Briner, J. P., Goehring, B. M., Mangerud, J., and Svendsen, J. I.: The deep accumulation of ^{10}Be at Utsira, southwestern Norway: implications for cosmogenic nuclide exposure dating in peripheral ice sheet landscapes, Geophys. Res. Lett., 43, 9121–9129, 2016.

Briner, J. P., Tulenko, J. P., Kaufman, D. S., Young, N. E., Baichtal, J. F., and Lesnek, A.: The last deglaciation of Alaska, Cuadernos de investigación geográfica/Geographical Research Letters, 43, 429–448, 2017.

Caissie, B. E., Brigham-Grette, J., Lawrence, K. T., Herbert, T. D., and Cook, M. S.: Last Glacial Maximum to Holocene sea surface conditions at Umnak Plateau, Bering Sea, as inferred from diatom, alkenone, and stable isotope records, Paleoceanography, 25, PA1206, https://doi.org/10.1029/2008PA001671, 2010.

Capps, S. R.: Glaciation in Alaska, United States Geological Survey, Reston, VA, Report 170A, https://doi.org/10.3133/pp170A, 1932.

Carrara, P. E., Ager, T. A., Baichtal, J. F., and VanSistine, D. P.: Map of glacial limits and possible refugia in the southern Alexander Archipelago, Alaska, during the late Wisconsin glaciation, United States Geological Survey, Reston, VA, Report 2424, 2003.

Carrara, P. E., Ager, T. A., and Baichtal, J. F.: Possible refugia in the Alexander Archipelago of southeastern Alaska during the late Wisconsin glaciation, Can. J. Earth Sci., 44, 229–244, https://doi.org/10.1139/e06-081, 2007.

Clague, J. J., Mathewes, R. W., and Warner, B. G.: Late Quaternary geology of eastern Graham Island, Queen Charlotte Islands, British Columbia, Can. J. Earth Sci., 19, 1786–1795, https://doi.org/10.1139/e82-157, 1982.

Clark, P. U., Dyke, A. S., Shakun, J. D., Carlson, A. E., Clark, J., Wohlfarth, B., Mitrovica, J. X., Hostetler, S. W., and McCabe, A. M.: The last glacial maximum, Science, 325, 710–714, 2009.

Cook, J. A., Bidlack, A. L., Conroy, C. J., Demboski, J. R., Fleming, M. A., Runck, A. M., Stone, K. D., and MacDonald, S. O.: A phylogeographic perspective on endemism in the Alexander Archipelago of southeast Alaska, Biol. Conserv., 97, 215–227, https://doi.org/10.1016/S0006-3207(00)00114-2, 2001.

Corbett, L. B., Bierman, P. R., and Rood, D. H.: An approach for optimizing in situ cosmogenic ^{10}Be sample preparation, Quat. Geochronol., 33, 24–34, https://doi.org/10.1016/j.quageo.2016.02.001, 2016.

Cosma, T. N., Hendy, I. L., and Chang, A. S.: Chronological constraints on Cordilleran Ice Sheet glaciomarine sedimentation from core MD02-2496 off Vancouver Island (western Canada), Quaternary Sci. Rev., 27, 941–955, https://doi.org/10.1016/j.quascirev.2008.01.013, 2008.

Dalton, A. S., Margold, M., Stokes, C. R., Tarasov, L., Dyke, A. S., Adams, R. S., Allard, S., Arends, H. E., Atkinson, N., Attig, J. W., Barnett, P. J., Barnett, R. L., Batterson, M., Bernatchez, P., Borns, H. W., Breckenridge, A., Briner, J. P., Brouard, E., Campbell, J. E., Carlson, A. E., Clague, J. J., Curry, B. B., Daigneault, R.-A., Dubé-Loubert, H., Easterbrook, D. J., Franzi, D. A., Friedrich, H. G., Funder, S., Gauthier, M. S., Gowan, A. S., Harris, K. L., Hétu, B., Hooyer, T. S., Jennings, C. E., Johnson, M. D., Kehew, A. E., Kelley, S. E., Kerr, D., King, E. L., Kjeldsen, K. K., Knaeble, A. R., Lajeunesse, P., Lakeman, T. R., Lamothe, M., Larson, P., Lavoie, M., Loope, H. M., Lowell, T. V., Lusardi, B. A., Manz, L., McMartin, I., Nixon, F. C., Occhietti, S., Parkhill, M. A., Piper, D. J. W., Pronk, A. G., Richard, P. J. H., Ridge, J. C., Ross, M., Roy, M., Seaman, A., Shaw, J., Stea, R. R., Teller, J. T., Thompson, W. B., Thorleifson, L. H., Utting, D. J., Veillette, J. J., Ward, B. C., Weddle, T. K., and Wright, H. E.: An updated radiocarbon-based ice margin chronology for the last deglaciation of the North Amer-

ican Ice Sheet Complex, Quaternary Sci. Rev., 234, 106223, https://doi.org/10.1016/j.quascirev.2020.106223, 2020.

Darvill, C. M., Menounos, B., Goehring, B. M., Lian, O. B., and Caffee, M. W.: Retreat of the western Cordilleran ice sheet margin during the last deglaciation, Geophys. Res. Lett., 45, 9710–9720, 2018.

Davies, M. H., Mix, A. C., Stoner, J. S., Addison, J. A., Jaeger, J., Finney, B., and Wiest, J.: The deglacial transition on the southeastern Alaska Margin: Meltwater input, sea level rise, marine productivity, and sedimentary anoxia, Palaeogeogr. Palaeocl., 26, PA2223, https://doi.org/10.1029/2010pa002051, 2011.

Demboski, J. R., Stone, K. D., and Cook, J. A.: Further perspectives on the Haida Gwaii glacial refugium, Evolution, 53, 2008–2012, https://doi.org/10.1111/j.1558-5646.1999.tb04584.x, 1999.

Dyke, A. S.: An outline of North American deglaciation with emphasis on central and northern Canada, Developments in Quaternary Sciences, 2, 373–424, 2004.

Eberlein, G. D., Churkin, M., Carter, C., Berg, H., and Ovenshine, A.: Geology of the Craig quadrangle, Alaska, United States Geological Survey, Reston, VA, Report 83-91, https://doi.org/10.3133/ofr8391, 1983.

Faure, G.: Principles of isotope geology, 2nd edition, Wiley, ISBN 978-0471864127, 1986.

Gosse, J. C. and Phillips, F. M.:. Terrestrial in situ cosmogenic nuclides: theory and application. Quaternary Sci. Rev., 20, 1475–1560, 2001.

Gregoire, L. J., Otto-Bliesner, B., Valdes, P. J., and Ivanovic, R.: Abrupt Bølling warming and ice saddle collapse contributions to the Meltwater Pulse 1a rapid sea level rise, Geophys. Res. Lett., 43, 9130–9137, 2016.

Hansen, B. C. S. and Engstrom, D. R.: Vegetation history of Pleasant Island, southeastern Alaska, since 13 000 yr BP, Quaternary Res., 46, 161–175, 1996.

Hebda, C. F. G., McLaren, D., Mackie, Q., Fedje, D., Pedersen, M. W., Willerslev, E., Brown, K. J., and Hebda, R. J.: Late Pleistocene palaeoenvironments and a possible glacial refugium on northern Vancouver Island, Canada: Evidence for the viability of early human settlement on the northwest coast of North America, Quaternary Sci. Rev., 279, 107388, https://doi.org/10.1016/j.quascirev.2022.107388, 2022.

Ivanovic, R. F., Gregoire, L. J., Wickert, A. D., Valdes, P. J., and Burke, A.: Collapse of the North American ice saddle 14 500 years ago caused widespread cooling and reduced ocean overturning circulation, Geophys. Res. Lett., 44, 383–392, 2017.

Jones, R. S., Whitehouse, P. L., Bentley, M. J., Small, D., and Dalton, A. S.: Impact of glacial isostatic adjustment on cosmogenic surface-exposure dating, Quaternary Sci. Rev., 212, 206–212, 2019.

Kienast, S. S. and McKay, J. L.: Sea surface temperatures in the subarctic northeast Pacific reflect millennial-scale climate oscillations during the last 16 kyrs, Geophys. Res. Lett., 28, 1563–1566, 2001.

Lal, D.: Cosmic ray labeling of erosion surfaces: in situ nuclide production rates and erosion models, Earth Planet. Sc. Lett., 104, 424–439, 1991.

Lesnek, A. J., Briner, J. P., Lindqvist, C., Baichtal, J. F., and Heaton, T. H.: Deglaciation of the Pacific coastal corridor directly preceded the human colonization of the Americas, Sci. Adv., 4, eaar5040, https://doi.org/10.1126/sciadv.aar5040, 2018.

Lesnek, A. J., Briner, J. P., Baichtal, J. F., and Lyles, A. S.: New constraints on the last deglaciation of the Cordilleran Ice Sheet in coastal Southeast Alaska, Quaternary Res., 96, 140–160, 2020.

Licciardi, J. M., Denoncourt, C. L., and Finkel, R. C.: Cosmogenic ^{36}Cl production rates from Ca spallation in Iceland, Earth Planet. Sci. Lett., 267, 365–377, https://doi.org/10.1016/j.epsl.2007.11.036, 2008.

Maier, E., Zhang, X., Abelmann, A., Gersonde, R., Mulitza, S., Werner, M., Méheust, M., Ren, J., Chapligin, B., and Meyer, H.: North Pacific freshwater events linked to changes in glacial ocean circulation, Nature, 559, 241–245, 2018.

Mann, D.H.: Wisconsin and Holocene glaciation of southeast Alaska, in: Glaciation in Alaska, edited by: Hamilton, T. D., Reed, K. M., and Thorson, R. B., Alaska Geological Society, Anchorage, AK, 237–265, B0018475H8, 1986.

Mann, D. H. and Hamilton, T. D.: Late Pleistocene and Holocene Paleoenvironments of the Pacific Coast, Quaternary Sci. Rev., 14, 449–471, https://doi.org/10.1016/0277-3791(95)00016-i, 1995.

Mann, D. H. and Peteet, D. M.: Extent and Timing of the Last Glacial Maximum in Southwestern Alaska, Quaternary Res., 42, 136–148, https://doi.org/10.1006/qres.1994.1063, 1994.

Marrero, S. M., Phillips, F. M., Caffee, M. W., and Gosse, J. C.: CRONUS-Earth cosmogenic ^{36}Cl calibration, Quat. Geochronol., 31, 199–219, 2016.

Mathewes, R. W. and Clague, J. J.: Paleoecology and ice limits of the early Fraser glaciation (Marine Isotope Stage 2) on Haida Gwaii, British Columbia, Canada, Quaternary Res., 88, 277–292, https://doi.org/10.1017/qua.2017.36, 2017.

Menounos, B., Goehring, B. M., Osborn, G., Margold, M., Ward, B., Bond, J., Clarke, G. K. C., Clague, J. J., Lakeman, T., Koch, J., Caffee, M. W., Gosse, J., Stroeven, A. P., Seguinot, J., and Heyman, J.: Cordilleran Ice Sheet mass loss preceded climate reversals near the Pleistocene Termination, Science, 358, 781–784, https://doi.org/10.1126/science.aan3001, 2017.

Miller, R. D.: Gastineau channel formation: a composite glaciomarine deposit near Juneau, Alaska, United States Geological Survey, Reston, VA, Bulletin 1394-C, 1973.

Misarti, N., Finney, B. P., Jordan, J. W., Maschner, H. D. G., Addison, J. A., Shapley, M. D., Krumhardt, A., and Beget, J. E.: Early retreat of the Alaska Peninsula Glacier Complex and the implications for coastal migrations of First Americans, Quaternary Sci. Rev., 48, 1–6, https://doi.org/10.1016/j.quascirev.2012.05.014, 2012.

Molnia, B. F.: Glaciers of North America – Glaciers of Alaska, United States Geological Survey, Reston, VA, Report 1386K, https://doi.org/10.3133/pp1386K, 2008.

Nishiizumi, K., Imamura, M., Caffee, M. W., Southon, J. R., Finkel, R. C., and McAninch, J.: Absolute calibration of ^{10}Be AMS standards, Nucl. Instrum. Meth. B, 258, 403–413, https://doi.org/10.1016/j.nimb.2007.01.297, 2007.

Porter, S. C. and Swanson, T. W.: Radiocarbon age constraints on rates of advance and retreat of the Puget lobe of the Cordilleran ice sheet during the last glaciation, Quaternary Res., 50, 205–213, 1998.

Praetorius, S., Mix, A., Jensen, B., Froese, D., Milne, G., Wolhowe, M., Addison, J., and Prahl, F.: Interaction between climate, volcanism, and isostatic rebound in Southeast Alaska during the last deglaciation, Earth Planet. Sc. Lett., 452, 79–89, 2016.

Praetorius, S. K. and Mix, A. C.: Synchronization of North Pacific and Greenland climates preceded abrupt deglacial warming, Science, 345, 444–448, 2014.

Praetorius, S. K., Mix, A. C., Walczak, M. H., Wolhowe, M. D., Addison, J. A., and Prahl, F. G.: North Pacific deglacial hypoxic events linked to abrupt ocean warming, Nature, 527, 362–366, 2015.

Reger, R. D., Pinney, D. S., Burke, R. M., and Wiltse, M. A.: Catalog and initial analyses of geologic data related to middle to late Quaternary deposits, Cook Inlet region, Alaska, State of Alaska Division of Geological and Geophysical Surveys Report of Investigations, 95–96, https://doi.org/10.14509/2520, 1996.

Riehle, J. R.: The Mount Edgecumbe Volcanic Field: A Geologic History, US Department of Agriculture, Forest Service, Alaska Region, https://avo.alaska.edu/downloads/reference.php?citid=639 (last access: 5 April 2022), 1996.

Riehle, J. R., Brew, D. A., Reed, K. M., and Bartsch-Winkler, S.: Explosive latest Pleistocene (?) and Holocene activity of the Mount Edgecumbe volcanic field, Alaska, US Geological Survey Circular, 939, 111–114, 1984.

Riehle, J. R., Champion, D. E., Brew, D. A., and Lanphere, M. A.: Pyroclastic deposits of the Mount Edgecumbe volcanic field, southeast Alaska: eruptions of a stratified magma chamber, J. Volcanol. Geoth. Res., 53, 117–143, 1992.

Seguinot, J., Khroulev, C., Rogozhina, I., Stroeven, A. P., and Zhang, Q.: The effect of climate forcing on numerical simulations of the Cordilleran ice sheet at the Last Glacial Maximum, The Cryosphere, 8, 1087–1103, https://doi.org/10.5194/tc-8-1087-2014, 2014.

Seguinot, J., Rogozhina, I., Stroeven, A. P., Margold, M., and Kleman, J.: Numerical simulations of the Cordilleran ice sheet through the last glacial cycle, The Cryosphere, 10, 639–664, https://doi.org/10.5194/tc-10-639-2016, 2016.

Shafer, A. B., Cullingham, C. I., Cote, S. D., and Coltman, D. W.: Of glaciers and refugia: a decade of study sheds new light on the phylogeography of northwestern North America, Mol. Ecol., 19, 4589–4621, https://doi.org/10.1111/j.1365-294X.2010.04828.x, 2010.

Shafer, A. B. A., White, K. S., Côté, S. D., and Coltman, D. W.: Deciphering translocations from relicts in Baranof Island mountain goats: is an endemic genetic lineage at risk?, Conserv. Genet., 12, 1261–1268, https://doi.org/10.1007/s10592-011-0227-8, 2011.

Shakun, J. D., Clark, P. U., He, F., Marcott, S. A., Mix, A. C., Liu, Z., Otto-Bliesner, B., Schmittner, A., and Bard, E.: Global warming preceded by increasing carbon dioxide concentrations during the last deglaciation, Nature, 484, 49–54, 2012.

Spratt, R. M. and Lisiecki, L. E.: A Late Pleistocene sea level stack, Clim. Past, 12, 1079–1092, https://doi.org/10.5194/cp-12-1079-2016, 2016.

Staiger, J., Gosse, J., Toracinta, R., Oglesby, B., Fastook, J., and Johnson, J. V.: Atmospheric scaling of cosmogenic nuclide production: climate effect, J. Geophys. Res.-Sol. Ea., 112, B02205, https://doi.org/10.1029/2005JB003811, 2007.

Stone, J. O., Allan, G. L., Fifield, L. K., and Cresswell, R. G.: Cosmogenic chlorine-36 from calcium spallation, Geochim. Cosmochim. Ac., 60, 679–692, https://doi.org/10.1016/0016-7037(95)00429-7, 1996.

Tarasov, L., Dyke, A. S., Neal, R. M., and Peltier, W. R.: A data-calibrated distribution of deglacial chronologies for the North American ice complex from glaciological modeling, Earth Planet. Sc. Lett., 315–316, 30–40, https://doi.org/10.1016/j.epsl.2011.09.010, 2012.

Taylor, M. A., Hendy, I. L., and Pak, D. K.: Deglacial ocean warming and marine margin retreat of the Cordilleran Ice Sheet in the North Pacific Ocean, Earth Planet. Sc. Lett., 403, 89–98, https://doi.org/10.1016/j.epsl.2014.06.026, 2014.

Walczak, M. H., Mix, A. C., Cowan, E. A., Fallon, S., Fifield, L. K., Alder, J. R., Du, J., Haley, B., Hobern, T., and Padman, J.: Phasing of millennial-scale climate variability in the Pacific and Atlantic Oceans, Science, 370, 716–720, 2020.

Warner, B. G., Mathewes, R. W., and Clague, J. J.: Ice-free conditions on the Queen Charlotte Islands, British Columbia, at the height of late Wisconsin glaciation, Science, 218, 675–677, 1982.

Wilcox, P. S., Dorale, J. A., Baichtal, J. F., Spotl, C., Fowell, S. J., Edwards, R. L., and Kovarik, J. L.: Millennial-scale glacial climate variability in Southeastern Alaska follows Dansgaard-Oeschger cyclicity, Sci. Rep., 9, 7880, https://doi.org/10.1038/s41598-019-44231-1, 2019.

Wilson, F. H., Hults, C. P., Mull, C. G., and Karl, S. M.: Geologic map of Alaska, US Department of the Interior, US Geological Survey, https://doi.org/10.3133/gip168, 2015.

Young, N. E., Schaefer, J. M., Briner, J. P., and Goehring, B. M.: A ^{10}Be production-rate calibration for the Arctic, J. Quaternary Sci., 28, 515–526, 2013.